

UC Berkeley

UC Berkeley Previously Published Works

Title

Practical design considerations for secondary air injection in wood-burning cookstoves: An experimental study

Permalink

<https://escholarship.org/uc/item/8pc507q0>

Authors

Caubel, Julien J
Rapp, Vi H
Chen, Sharon S
et al.

Publication Date

2020

DOI

10.1016/j.deveng.2020.100049

Peer reviewed

1
2
3
4
5
6
7
8
9
10
11
12
13
14
15

Practical Design Considerations for Secondary Air Injection in Wood-Burning Cookstoves: An Experimental Study

Julien J. Caubel†‡, Vi H. Rapp‡, Sharon S. Chen‡, Ashok J. Gadgil‡¶*

† Department of Mechanical Engineering, University of California, Berkeley, Berkeley,
California 94720, United States

‡ Environmental Technologies Area, Lawrence Berkeley National Laboratory, Berkeley,
California 94720, United States

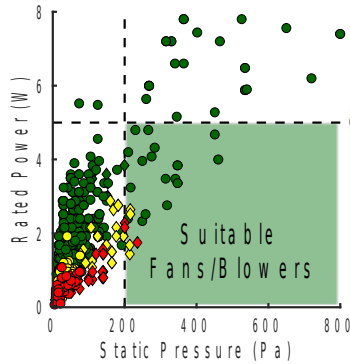
¶ Department of Civil and Environmental Engineering, University of California, Berkeley,
Berkeley, California 94720, United States

**1 Cyclotron Road MS 90R2121, Berkeley, CA 94720*

Phone: 01-510-495-2035; E-mail: jcaubel@berkeley.edu

16

17 **Abstract**



18

(TOC Art)

19 Billions of households worldwide cook using biomass fires and suffer from the toxic
20 smoke emitted into their homes. Laboratory studies of wood-burning cookstoves demonstrate
21 that secondary air injection can greatly reduce the emission of harmful air pollution, but these
22 experimental advancements are not easily translated into practical cookstove designs that can be
23 widely adopted. In this study, we use a modular cookstove platform to experimentally quantify
24 the practical secondary air injection design requirements (e.g., flow rate, pressure, and
25 temperature) to reduce mass emissions of particulate matter (PM), carbon monoxide (CO), and
26 black carbon (BC) by at least 90% relative to a traditional cooking fire. Over the course of 111
27 experimental trials, we illuminate the physical mechanisms that drive emission reductions, and
28 outline fundamental design principles to optimize cookstove performance. Using the
29 experimental data, we demonstrate that low-cost (<\$10) fans and blowers are available to drive
30 the secondary flow, and can be independently powered using an inexpensive thermoelectric
31 generator mounted nearby. Furthermore, size-resolved PM measurements show that secondary
32 air injection inhibits particle growth, but the total number of particles generated remains

33 relatively unaffected. We discuss the potential impacts for human health and investigate methods
34 to mitigate the PM formation mechanisms that persist.

35 **Keywords:** biomass cookstove; household energy; air pollution; design; combustion

36 **1. Introduction**

37 Over 2 billion people cook using solid biomass fuels, such as wood and dung.^{1,2}
38 Typically, households rely on traditional biomass cookstoves that are highly inefficient and
39 polluting.^{3,4} When these cookstoves are used in poorly ventilated homes, indoor concentrations of
40 harmful pollutants, such as particulate matter (PM) and carbon monoxide (CO), can be up to 100
41 times higher than levels recommended by the World Health Organization (WHO).⁵⁻⁷

42 As a result, chronic exposure to indoor air pollution from solid biomass cookstoves is a
43 leading environmental health risk, causing nearly 2 million premature deaths annually.^{8,9}

44 Some biomass cookstoves are designed to reduce unwanted emissions by using a small
45 fan or blower to inject secondary air into the combustion chamber.¹⁰⁻¹⁴ When properly injected,
46 the jets of secondary air increase the turbulent mixing and residence time of gas-phase fuel in the
47 combustion zone, while providing oxygen directly to fuel-rich regions.¹⁵⁻²¹ As a result, fuel
48 oxidation is more complete, fewer harmful pollutants are emitted, and thermal efficiency is
49 enhanced.^{14,15} However, secondary air is typically much cooler than the exhaust gases and
50 improper injection can result in lower combustion temperatures that limit fuel oxidation and heat
51 transfer to the thermal load (e.g. a cooking pot).¹⁹⁻²³ For example, Jetter et al. evaluated the
52 performance of several secondary air injection cookstoves and showed that half do not reduce
53 PM or CO mass emissions relative to a three stone fire (TSF).¹⁰

54 Studies have shown that many secondary air injection design parameters, such as the flow
55 rate and geometry, must be carefully considered and validated in order to significantly reduce
56 unwanted emissions from biomass combustion appliances.^{15,16,19-21,23-25} However, current studies
57 do not usually consider the critical operational parameters needed to appropriately size the core

58 components of a practical, stand-alone cookstove. For example, no information is provided on
59 the positive pressure required to drive the secondary air injection flow, although this information
60 is required to select fans or blowers. Consequently, emission reductions achieved in the
61 laboratory are not easily translated into cookstove designs that can be manufactured, distributed,
62 and adopted on a large scale.

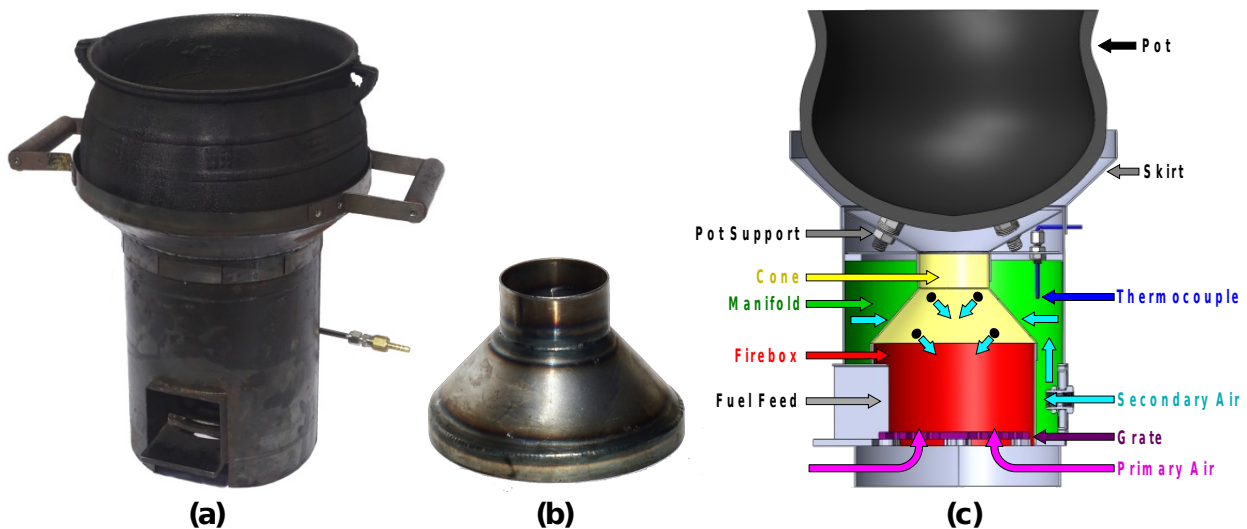
63 In this study, we use an experimental cookstove platform to investigate the practical
64 secondary air injection design requirements for reducing the mass emission of air pollutants from
65 unprocessed wood combustion by one order of magnitude. We conducted 111 experimental
66 trials, systematically varying critical secondary air injection parameters (e.g. flow rate and
67 location) to identify a design configuration that emits 90% less CO, PM, and (BC) than a TSF,
68 and also improves thermal efficiency. We targeted mass emission reductions of at least 90%
69 because indoor pollution concentrations from traditional biomass cooking easily exceed health
70 guidelines by 10 times or more.^{3,6,7,26} Throughout the experimental optimization, we recorded the
71 secondary air injection flow rate, pressure and temperature to evaluate whether the performance
72 improvements are practically achievable using inexpensive, off-the-shelf components that can be
73 powered independently (e.g., small fans powered by a thermoelectric generator). Furthermore,
74 we use size-resolved PM measurements to investigate the underlying physical mechanisms
75 contributing to the reduction of total PM mass emissions and identify particle size ranges where
76 further emission reductions are needed.

77

78 **2. Materials and Methods**

79 **2.1 Modular Air Injection Cookstove Design: Version 2 (MOD2)**

80 The MOD2 stove, presented in Figure 1, is a continuously fed, wood-burning cookstove
 81 that enables critical secondary air injection parameters to be modulated easily and repeatedly.
 82 The MOD2 stove is the second design iteration of the modular (MOD) stove described by
 83 Caubel et al.,²⁰ and therefore shares the same general design architecture and accommodates the
 84 same cast-aluminum Darfuri cooking pot. The MOD2 stove has a cylindrical firebox, 15 cm (6
 85 inch) in diameter, with an open fuel feed at the front. Primary air enters the firebox through the
 86 open fuel feed, and adjustable openings below the grate. Above the firebox, a conical chimney
 87 reduces to a 6.4-cm (2.5-inch) diameter throat located directly below the pot. An integrated air
 88 manifold surrounds the firebox and conical chimney assembly (Figure 1(c)). Secondary air is
 89 supplied to a port at the back of the manifold and is injected into the firebox through orifices
 90 drilled into the conical chimney. The conical chimney is removable, such that different air
 91 injection patterns can easily be drilled, installed, and tested (Figure 1(b)). The pot's height above
 92 the chimney throat is controlled using adjustable supports. The stove also incorporates a steel
 93 skirt that closely surrounds the pot to enhance the rate of heat transfer from the exhaust gases.



95 **Figure 1.** (a) The MOD2 stove with cast-aluminum Darfuri pot; (b) Removable conical chimney,
96 into which secondary air injection patterns are drilled; (c) Cross-sectional view of the MOD2
97 stove showing the firebox, conical chimney, secondary air manifold, secondary air flow path, and
98 other design features. Air injection holes are enlarged (out of scale) for clarity.

99 Previous research on the MOD stove (version 1) demonstrated that higher secondary air
100 injection velocities improved stove performance, but excessive secondary flow quenched the
101 combustion.²⁰ The velocity of the secondary air jets decreases rapidly after injection into the
102 firebox. For the 1.59-mm (0.0625-inch) diameter secondary air injection orifices used throughout
103 the MOD stove (version 1) study, the average jet velocity diminishes by 90% over a normal
104 distance of just 4 cm,^{27,28} or less than half of the distance required to reach the center of the MOD
105 stove's firebox. To ensure that secondary air jets better reach the flames, the MOD2 stove's
106 firebox and conical chimney diameters are approximately 15% smaller than in the MOD stove.
107 By reducing the distance from the orifices to the combustion zone, the velocity of the air jets is
108 higher when they reach the flames, thereby promoting turbulent mixing and oxygen injection at
109 lower secondary flow rates that do not prohibitively cool the combustion. MOD2 stove
110 dimensions were not reduced further, as a 15-cm firebox was deemed to be the smallest size that
111 allows easy feeding and tending of the firewood. Additional details regarding the MOD2 stove
112 design are provided in the SI.

113

114 **2.2 Experimental Set-Up and Stove Testing Procedure**

115 The MOD2 stove was developed at Lawrence Berkeley National Laboratory's (LBNL)
116 cookstove testing facility. The experimental setup and testing procedure for the MOD2 stove are

117 the same as that described by Caubel et al. for the MOD stove (version 1),²⁰ and a brief overview
118 is provided here. During testing, emissions from the MOD2 stove are completely captured using
119 a steel hood, and exhausted outdoors using a steel ducting system and blowers. Air pollution
120 instruments sample the duct flow and provide emission concentration measurements every
121 second (1 Hz). A California Analytical Instruments 600 Series gas analyzer measures the
122 volumetric concentrations (ppmv) of CO, carbon dioxide (CO₂), and oxygen (O₂). The total mass
123 of PM_{2.5} (PM with aerodynamic diameter ≤ 2.5 μm) emitted during the test phase is measured
124 gravimetrically. A suite of real-time PM instruments sample emissions from the duct using a
125 secondary diluter. A TSI 3091 Fast Mobility Particle Sizer (FMPS) and a TSI 3321 Aerodynamic
126 Particle Sizer (APS) together provide size-resolved particle number concentration measurements
127 from 5 to 2500 nm, while a Magee Scientific AE-22 Aethalometer provides black carbon (BC)
128 mass concentration measurements. All instruments were calibrated according to manufacturer
129 recommendations, as described by Caubel et al.²⁰

130 The MOD2 stove was tested using the cold start, high power phase of the Water Boiling
131 Test (WBT) 4.2.3 as pollutant emissions are usually highest during this phase of stove use.^{20,29,30}

132 For each test, the MOD2 stove was initially at ambient temperature (“cold”), and a new
133 fire was lit in a cold fuel bed (kindling). The stove was fueled with Douglas Fir wood cut into
134 uniform 25 x 25 x 152-mm (1 x 1 x 6-inch) pieces and allowed to dry to 7-9% moisture content
135 on a wet basis. Wood pieces were fed into the combustion chamber lengthwise, with one end
136 slightly protruding from the open feed. The fuel feed rate was controlled to maintain a constant
137 firepower setting of ~5 kW (monitored using real-time CO₂ concentration measurements from the
138 exhaust duct) while bringing 5 L of cold water to a temperature of 99°C, the nominal local
139 boiling point. Secondary air came from a compressed air cylinder. The standard volumetric flow

140 rate (SLPM) of secondary air was measured using a rotameter, and adjusted using a valve. The
141 secondary air flow was initiated ~2 min after fuel ignition, once the kindling was observed to be
142 fully lit, and was held constant throughout the remainder of the test. The secondary air
143 temperature was monitored every second (1 Hz) using a thermocouple installed inside the stove
144 manifold (Figure 1(c)). Manifold pressures were measured with a digital manometer through a
145 dedicated tap.

146 **2.3 Parametric Testing Procedure**

147 Four MOD2 stove design parameters were systematically varied over a total of 111 tests:
148 (1) secondary air injection pattern (2) secondary air injection flow rate (3) primary air intake, and
149 (4) pot height. The first 52 tests were conducted to constrain the parametric space. Two
150 promising air injection patterns were identified during these preliminary tests, shown in Figure
151 A4 (a total of 7 patterns were tested). Pattern 1 consisted of two concentric rows, each with three
152 orifices evenly spaced around the circumference of the conical chimney. The bottom row of
153 orifices was located just above the firebox, while the top was directly below the throat. Pattern 2
154 was identical, except that the bottom row had six evenly spaced orifices, rather than three. All air
155 injection orifices had a diameter of 1.59 mm (0.0625 inch). The primary air intake (the size of the
156 inlet area under the grate) and pot height were also set during the preliminary tests, according to
157 the experimental procedures and results provided in the SI.

158 For the remaining 59 parametric tests, the primary air intake was set to the fully open
159 position and the pot height was held at 25 mm (except for the first 13 tests, when the pot was set
160 2 to 5 mm lower). Using these settings, both air injection patterns were tested at six secondary air
161 flow rate settings ranging from 14 to 50 SLPM (0.5 to 1.75 SCFM), for a total of 12 parametric
162 configurations. Four to eight replicate tests were conducted at each configuration (except for

163 Pattern 2 at 50 SLPM, with only 2 tests). When calculating configuration-average performance
164 and emission metrics using this number of replicate tests, corresponding two-sided 90%
165 confidence intervals were most often $< 20\%$ ($\pm 10\%$) of the configuration-average values. This
166 level of statistical confidence was deemed sufficient to enable meaningful comparisons. During
167 testing, we discovered that the stove's air manifold leaked at the juncture between the removable
168 conical chimney and the stove body (Figure A2). However, the leakage was consistent and
169 replicable, and so the secondary flow actually injected into the firebox could be accurately
170 calculated (see the procedure outlined in the SI). The calculations show that 27% to 39% of the
171 total secondary flow was injected through the holes in the conical chimney, while the remainder
172 leaked through the faulty manifold juncture, away from the firebox and combustion process. All
173 results are presented in terms of the standard flow rate (SLPM) of air injected into the firebox,
174 ranging from 5.5 to 14 SLPM, rather than the total flow into the manifold.

175

176 **2.4 Data Analysis and Performance Metrics**

177 All stove performance and emission metric calculations are presented in section S-1.4 of
178 the SI. Emission factors are normalized by the average thermal power delivered to the pot,
179 known as cooking power (kWd). All data are presented with 90% confidence intervals calculated
180 using Student's t-distribution.^{31,32} The MOD2 stove's performance and emissions are compared
181 to those of the MOD stove (version 1) and a TSF, both tested using the same experimental
182 procedure, fuel, cooking pot, and firepower setting (~ 5 kW).^{20,21} All size-resolved particle
183 emission measurements from the TSI 3321 APS are converted from aerodynamic to electrical
184 mobility diameter, and combined with measurements from the TSI 3091 FMPS according to the
185 methods outlined in Appendix A.

186 For both air injection patterns, the manifold pressure was measured at each secondary
187 flow rate setting while the stove was cold, as described in Appendix A. Using real-time manifold
188 temperature measurements and Equation 1 below, stove manifold pressures during each test were
189 extrapolated from the corresponding pressure measurement recorded while the stove was cold.

$$190 \Delta P(t) = \Delta P_{STP} \left(\frac{\rho_{STP}}{\rho(t)} \right) = \frac{\Delta P_{STP} \rho_{STP} (T_{man}(t) + 273) R_{air}}{P_{man}} (1)$$

191 $\Delta P(t)$ (Pa) is the manifold gauge pressure at sample time 't', ΔP_{STP} (Pa) is the manifold gauge
192 pressure measured at ambient conditions (shown in Figure A6), ρ_{STP} is the density of air at
193 standard conditions (1.225 kg/m³), $T_{man}(t)$ (°C) is the air temperature in the manifold at sample
194 time 't', R_{air} is the ideal gas constant for air (287 J/Kg K), and P_{man} is the absolute pressure in the
195 manifold (roughly equal to the local ambient pressure, 97150 Pa). Average manifold pressures
196 represent the mean of all one-second values calculated over the length of the cold start test.

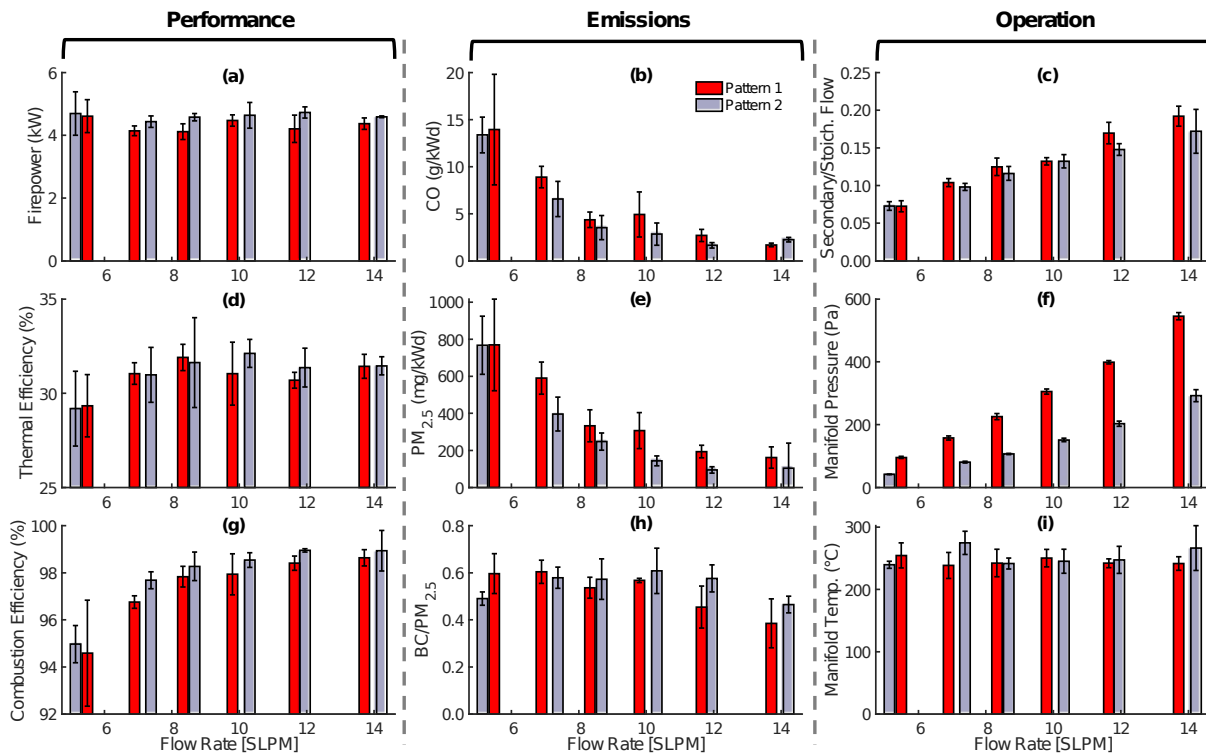
197

198 **3. Results and Discussion**

199 **3.1 Stove Performance and Emissions: Air Injection Pattern and Flow Rate**

200 For both air injection patterns, Figure 2 shows that the MOD2 stove's thermal and
201 emissions performance improve significantly as the secondary flow rate increases from 5.3 to 8.5
202 SLPM. Since firepower was held constant throughout testing, the average stoichiometric flow of
203 air into the combustion reaction is ~70 SLPM for all design configurations (Figure B4), and the
204 total flow of air through the stove may be 2-5 times higher than this stoichiometric value, as the
205 wood combustion draws excess primary air.^{24,33,34} Over this range of secondary flow rates, which
206 account for 7.5 to 12% of the average stoichiometric air flow, CO, PM_{2.5}, and BC emissions drop
207 by 55% to 75%, while combustion efficiency rises from 95% to 98%. These improvements

208 demonstrate that unprocessed wood combustion is highly sensitive to small changes in secondary
 209 flow (relative to the total combustion flow), as higher air jet velocities provide more turbulent
 210 mixing and oxygen in the combustion zone.¹⁸ The improvement of combustion conditions also
 211 translates to gains in thermal efficiency, which increases from 29% to 32% over this range.



212
 213 **Figure 2.** MOD2 stove performance, emissions, and operational metrics during high-power cold
 214 start testing, presented as function of secondary air injection pattern and flow rate: (a) Firepower
 215 (kW); (b) Carbon Monoxide (CO) emissions (g/kWd); (c) Ratio of the secondary to
 216 stoichiometric flow rate of air; (d) Thermal efficiency (%); (e) Particulate matter (PM_{2.5})
 217 emissions (mg/kWd); (f) Average manifold pressure (Pa); (g) Combustion efficiency (%); (h)
 218 Black Carbon (BC) to total PM_{2.5} ratio; (i) Average manifold temperature (°C). Bars represent
 219 the mean of replicate test data collected for each stove configuration, while error bars represent
 220 the corresponding 90% confidence interval.

221 For secondary flow rates above 8.5 SLPM, thermal efficiency remains constant around
222 31%. At these settings, the secondary flow represents 12 to 18% of the average stoichiometric
223 flow of air and is much colder than the exhaust gases. The average manifold temperature is
224 roughly 250 °C for all configurations, while exhaust temperatures from biomass combustion
225 typically exceed 850 °C.^{16,24} Although the secondary air represents a small fraction of the total air
226 flow into the stove, it may be sufficient at these settings (> 8.5 SLPM) to cool the exhaust gases
227 appreciably, thereby limiting the rate of heat transfer to the pot. Other biomass cookstove studies
228 show that exhaust temperatures drop with increased secondary flow.^{16,22,35}

229 Some of the fire's thermal power output is also used to heat the secondary air in the
230 manifold. Since average secondary air temperatures remain approximately constant for all
231 configurations, more heat from the fire is necessarily transferred to the manifold as secondary
232 flow increases. However, Figure B4 shows that less than 0.1 kW is lost to heating the secondary
233 air at all flow rates, which is small compared to the average thermal power delivered to the pot
234 (~1.4 kW). Therefore, secondary flow does not need to be constrained to maintain high air
235 injection temperatures or prevent the diversion of output heat from the pot to the secondary air
236 manifold, though some restraint is required to prevent excessive cooling of the exhaust gases.

237 Although thermal performance gains diminish with secondary flow rates above 8.5
238 SLPM, CO, PM_{2.5}, and BC emissions generally decrease steadily throughout the parametric
239 range (Figure 2 and Figure B4), thereby suggesting that combustion temperatures remain
240 sufficiently elevated to oxidize harmful pollutants, and higher air injection velocities continue to
241 enhance mixing of the air and gas-phase fuel. Correspondingly, combustion efficiency increases
242 from 98 to 99% as secondary flow rate increases above 8.5 SLPM, representing a further ~50%
243 reduction in the fraction of carbon emitted as a product of incomplete combustion (CO).

244 However, average emissions of CO and PM_{2.5} from Pattern 2 increase slightly at a flow rate of 14
245 SLPM. While only two tests were conducted in this configuration, the results suggest that
246 secondary flow rates above 12 SLPM through Pattern 2 may quench the flames, and reduce
247 combustion zone temperatures below the 850 °C required to oxidize CO and many of the volatile
248 organic species that form PM.^{16,18,22} However, BC emissions continue to decrease in this stove
249 configuration, as the oxidation temperature of BC is much lower (~350 °C) than that of CO and
250 other pollutants,^{36,37} and higher air injection velocities inhibit the formation of fuel-rich flame
251 zones where BC is formed.^{38,39}

252 Emission reductions are not solely dependent on higher secondary air injection velocities
253 to enhance the combustion process. At each flow rate setting, the average injection velocity is
254 roughly 1.5 times greater through Pattern 1 than Pattern 2 (Figure B4), and yet Figure 2 shows
255 that Pattern 2 generally outperforms Pattern 1. This trend suggests that the addition of air jets
256 near the fuel bed promotes more effective turbulent mixing in the combustion zone, despite the
257 drop in injection velocity. In this way, wood combustion is also highly sensitive to the number of
258 secondary air injection orifices and their location relative to the fuel bed, and this sensitivity can
259 be exploited to enhance stove performance. For example, Figure 2 shows that the manifold
260 pressure at each flow rate setting is 1.9 to 2.3 times lower for Pattern 2 than for Pattern 1
261 (theoretically, the manifold pressure should be 2.25 times lower, as the air injection area 1.5
262 times greater). As a result, greater performance improvements are possible using lower
263 secondary flow rates and pressures that can be more easily provided by the miniature fans and
264 blowers typically found in improved cookstoves.

265 Figure 2 shows that a secondary flow rate of 12 SLPM through Pattern 2 minimizes the
266 MOD2 stove's CO and PM_{2.5} emissions, while maximizing combustion efficiency. Although

267 thermal efficiency and BC emissions improve slightly ($\leq 10\%$ relative change) at other flow rate
268 settings, this configuration likely provides an optimal balance between reducing harmful
269 emissions and improving thermal performance. In this configuration, the MOD2 stove emits 90%
270 less CO, PM_{2.5}, and BC than a TSF (on average), and thermal efficiency increases from 23±1% to
271 31±1% (Table S1).

272 While the MOD2 stove can be optimized to reduce biomass smoke emissions by roughly
273 one order of magnitude (relative to a TSF), the ratio of BC to total PM_{2.5} emissions ranges from
274 0.4 to 0.6 throughout the parametric range, which is higher than that typically reported for
275 biomass cookstoves, both traditional and improved.^{25,26,40,41} Initially, we suspected that these
276 unusually elevated BC emission measurements might be the result of instrumentation error,
277 although the Aethalometer was calibrated by the manufacturer prior to both experimental testing
278 phases. Using calibration factors from the manufacturer and fundamental equations, we correctly
279 replicated the instrument's BC concentration outputs from the underlying optical absorption and
280 sample flow rate measurements. During this validation process, we did not uncover any
281 indication that the instrument was operating incorrectly. Taken at face value, the high proportion
282 of BC detected in the MOD2 stove emissions indicates that incomplete oxidation conditions
283 persist.^{17,25,42} However, BC is readily oxidized, and can be mitigated through improvements in the
284 combustion process.⁴³ Therefore, it is important to identify the physical mechanisms responsible
285 for these BC emissions such that they can be actively targeted in future designs.

286 The BioLite™ HomeStove™ is a wood-burning cookstove similar to the MOD2 stove
287 that emits ~80% less PM_{2.5} than the TSF presented here, and also has elevated BC/PM_{2.5} ratios
288 (>0.7).¹¹ These results suggest that rocket-style cookstoves with secondary air injection may
289 oxidize most PM-forming species, but BC generation somehow persists. A likely explanation for

290 these persistent BC emissions is that the water-filled cooking pot is quenching flames protruding
291 from the chimney throat.⁴⁴ When the MOD2 stove was operated without a pot skirt during
292 preliminary tests, Figures B1 and B4 show that PM_{2.5} emissions were comparable, but BC
293 emissions were 2 to 3 times lower. Therefore, the BC/PM_{2.5} ratio was significantly reduced
294 (<0.25), though thermal efficiency also suffered without the pot skirt (< 29%). The pot skirt
295 restricts the exhaust flow to enhance heat transfer, but the resultantly higher exhaust velocities
296 entrain more flames through the chimney throat, where fuel-rich zones quench against the pot
297 and emit BC. These results motivate further investigations that focus on preventing flame contact
298 with the pot to reduce BC emissions while maintaining high thermal efficiency.

299 Compared to the MOD stove (version 1), the MOD2 stove achieves similar emission
300 reductions at half the secondary air injection flow rate. Furthermore, when the secondary flow
301 rate was set 25% higher than the optimal setting, PM_{2.5} and CO emissions from the MOD stove
302 more than doubled.²⁰ MOD2 stove emissions, on the other hand, increase only slightly (<40%)
303 when the flow rate rises by ~17%, from 12 SLPM to 14 SLPM. Together, these trends illustrate
304 that the MOD2 stove's smaller firebox and chimney dimensions allow the secondary air jets to
305 be more effective at lower flow rates, penetrating further into the firebox to enable significant
306 emission reductions while preventing excessive cooling or quenching of the combustion.
307 Additionally, the lower secondary flow rates likely contribute to the MOD2 stove's higher
308 thermal efficiency, as cooling of the exhaust flow diminishes.

309 Together, the experimental results demonstrate that the secondary air injection pattern
310 and flow rate must be optimized to maximize the effective jet velocity but prevent flame
311 quenching. Design compromises are also sometimes required to enhance both the stove's thermal
312 and emissions performance. In this case, adding a pot skirt to the MOD2 stove enhanced thermal

313 efficiency but also increased the BC/PM_{2.5} ratio. Since the MOD2 stove still achieves significant
314 (90±10%) BC mass emission reductions relative to a TSF, the elevated BC/PM_{2.5} ratio may be
315 justified by the increase in thermal efficiency afforded. Having identified the optimal MOD2
316 stove design configuration and established the underlying physical mechanisms responsible for
317 the performance improvements, it is important to determine whether these experimental results
318 can be translated into a practical cookstove design that households can afford and adopt.

319

320 **3.2 Secondary Air Injection Design Requirements: Flow, Pressure and Power**

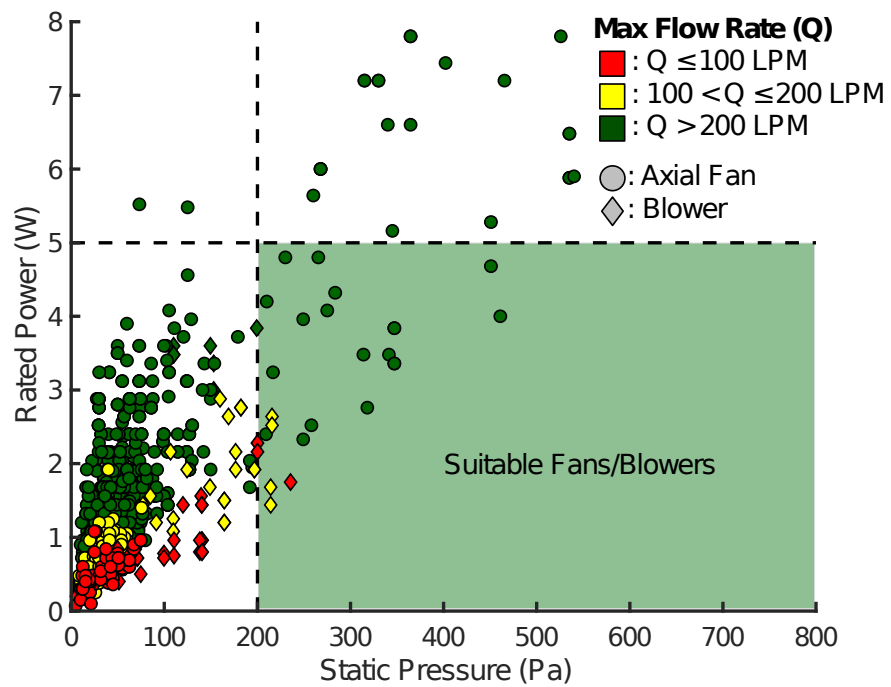
321 The MOD2 stove receives pressurized air from a cylinder, such that the secondary flow
322 can be adjusted accurately and consistently over the course of many experimental trials, but this
323 approach is clearly not practical or economical for typical household applications. Instead, many
324 commercial biomass cookstoves rely on a small axial fan or centrifugal blower to drive the
325 secondary flow, often drawing electrical power from a thermoelectric generator (TEG).^{11,14} TEGs
326 convert heat from the biomass combustion directly to electricity, thereby providing an
327 independent, reliable, and convenient source of power at little cost (often < \$10/W of power
328 generated).⁴⁵⁻⁴⁸ TEG modules mounted to biomass cookstoves have been shown to generate as
329 much as 10 W of electrical power, although an output of 1 to 5 W is more typical.^{45,47-49} There are
330 also some biomass cookstoves powered by solar panels or simple wall chargers, but these
331 alternatives are often less desirable, as they depend on operational factors external to the
332 cookstove (such as sufficient insolation).

333 Figure 2 shows that MOD2 performance is optimal when injecting a secondary flow rate
334 of 12 SLPM through Pattern 2. In this configuration, an average manifold pressure of ~200 Pa is
335 required. As the stove heats up during normal use, higher manifold pressure is required to

336 maintain a constant mass flow of secondary air through the injection pattern. Air is injected into
337 the MOD stove at room temperature (~25 to 30 °C) throughout, but reaches manifold
338 temperatures of 300 to 400 °C during the cold start test (Figure 5). The density of air at these
339 elevated temperatures is around half that of the air initially flowing into the manifold, and so the
340 volumetric flow rate passing through the injection pattern effectively doubles, as does the
341 manifold pressure required. Consequently, when sizing a fan or blower to drive secondary air
342 injection in a biomass cookstove, it is important to consider the manifold pressure required at
343 typical operating conditions, rather than when the stove is cold (at ambient temperature). In this
344 study, we defined the operating temperature as the average secondary air temperature in the
345 manifold during the cold start, and therefore we also present the average manifold pressure.

346 Figure 3 provides the maximum (static) pressure, maximum (free) flow rate, and rated
347 electrical power consumption of 1,135 miniature fans and blowers stocked by Digi-Key
348 Electronics®, a major electronic parts supplier.⁵⁰ This dataset is provided in Appendix B5. All
349 available models costing < \$10 (when ordering 1000 units) are presented, as the minimization of
350 manufacturing costs is crucial to the development of affordable cookstoves. To reflect the MOD2
351 stove's operational requirements, reference lines are provided at a static pressure of 200 Pa and
352 rated electrical power of 5 W (the maximum power typically output by a stove-mounted TEG
353 module). The devices must operate near static conditions, or at a flow rate below ~10% of the
354 maximum value specified by the manufacturer (measured with no flow resistance), to generate
355 the maximum pressures presented in Figure 3. The MOD2 stove requires 12 SLPM in the
356 optimal configuration, so the free flow rate should be at least ~100 LPM for the fan or blower to
357 operate near static conditions. This target is based on a rough approximation of actual
358 performance, so fans and blowers with a free flow rating ranging from 100 to 200 LPM (at

359 standard conditions) are represented using yellow markers (Figure 3) to indicate that some may
 360 not satisfy the 12 SLPM requirement under operational conditions. Green markers represent
 361 devices that are nearly certain to meet or exceed the stove's secondary flow rate requirement,
 362 while red markers indicate devices unlikely to meet the requirements. Since secondary air is
 363 drawn into the stove from the environment near standard conditions, the rated volumetric flow
 364 rate (LPM) is analogous to the stove's mass flow rate (SLPM) requirements, identified
 365 experimentally. It should also be noted that the rated power consumption is often measured at
 366 free flow conditions, and though this may not be exactly representative of power consumption at
 367 the requisite operating conditions (which will likely be larger as flow resistance is applied), it
 368 provides a valid estimate.



369
 370 **Figure 3.** Static pressure, free flow rate, and rated electrical power consumption of 1,135
 371 miniature axial fans and centrifugal blowers that are stocked by Digi-Key Electronics © and cost
 372 < \$10 per unit (when ordering 1000 units).⁵⁰ Fans and blowers that meet the MOD2 stove's

373 operational requirements (in the optimal design configuration) are indicated. Marker colors
374 represent the devices' ability to operate near static flow conditions while providing the stove's
375 required flow rate (12 SLPM).

376 Only 23 (~2%) of the 1,135 fans and blowers presented in Figure 3 meet the MOD2
377 stove's static pressure (>200 Pa), free flow (>100 SLPM), and electrical power (<5 W)
378 requirements. Miniature fans and blowers are typically designed for cooling electronics, and
379 therefore provide high air flow rates at low pressures – over 70% of the devices shown in Figure
380 3 generate maximum flow rates > 100 LPM using < 5 W of power, but at static pressures < 100
381 Pa. However, the MOD2 stove requires relatively low flow rates of air, driven through small
382 orifices that generate high velocity air jets in the combustion chamber, but require high input
383 pressures.

384 The small proportion of suitable fans and blowers illustrates the importance of carefully
385 characterizing the cookstove's operational requirements. Using only knowledge of the air
386 injection flow rate, as is usually provided in existing experimental studies, it is straightforward to
387 select a fan or blower that meets the flow requirement, but provides insufficient positive pressure.
388 Similarly, without manifold temperature measurements, it would be difficult to discern that the
389 cookstove's volumetric flow rate and manifold pressure requirements double during normal
390 operation. This analysis suggests that poorly performing cookstoves with secondary air injection
391 may suffer from the implementation of inadequate fans and blowers, as operational guidelines
392 are lacking.

393 Of the 23 viable devices identified, Figure 3 shows that suitable blowers generally
394 require less power than axial fans, as they are better suited to high pressure, low flow
395 applications. Overall, Figure 3 illustrates that low-cost fans and blowers are currently available
396 to achieve effective and practical secondary air injection in wood-burning cookstoves, but they
397 must be carefully chosen and evaluated, as the vast majority are not intended to meet the flow,
398 pressure, and electrical power consumption conditions required.

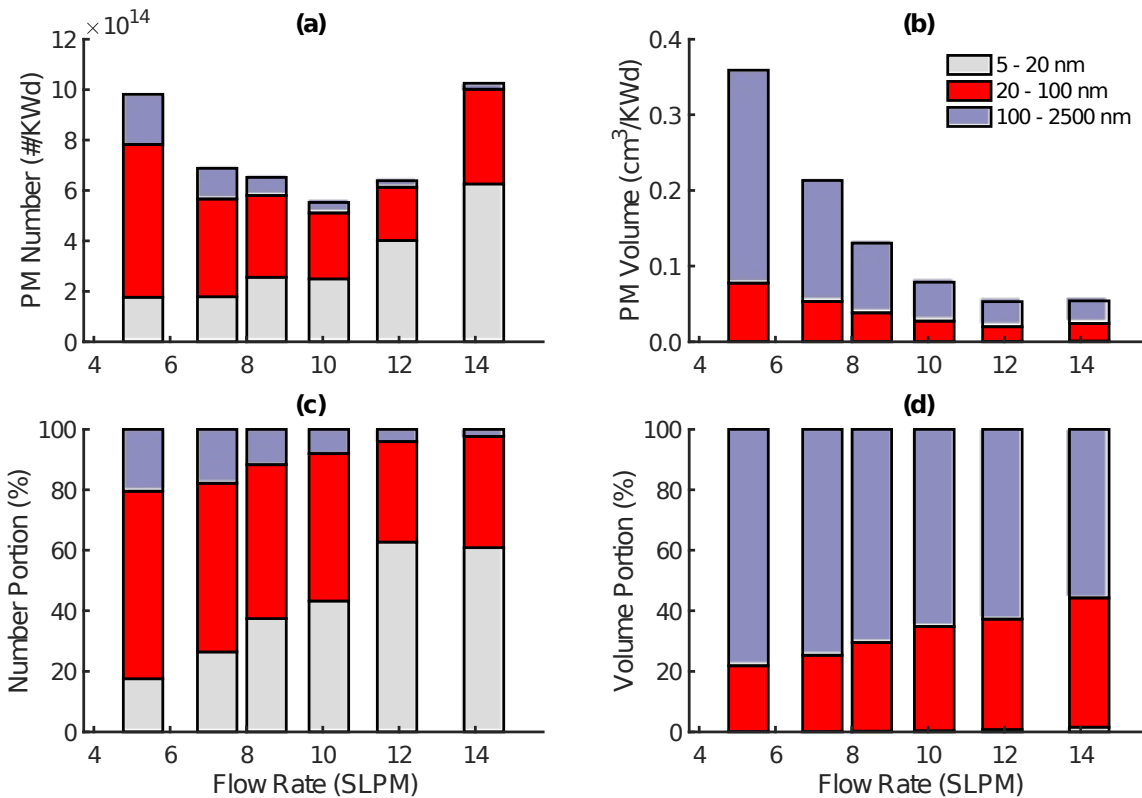
399

400 **3.3 Room for Improvement: Start Up and Ultrafine Particle Emissions**

401 Health guidelines from the WHO, United States Environmental Protection Agency (US
402 EPA), and other organizations generally recommend maximum PM_{2.5} pollution levels in terms of
403 mass concentration (e.g., µg/m³). By this measure, the MOD2 stove should alleviate health
404 impacts from biomass combustion, as it reduces PM_{2.5} mass emissions by an order of magnitude
405 relative to a traditional TSF. However, Figure 4 shows that the vast majority (>80%) of PM_{2.5}
406 emissions from the MOD2 stove consist of ultrafine particles (UFP) with a diameter < 100 nm,
407 which may be particularly harmful to human respiratory health, as their small size enables deeper
408 penetration into the lungs.⁵¹⁻⁵⁴ Consequently, it is important not only to reduce the mass of PM
409 generated, but also the number of UFPs emitted and potentially inhaled.

410 Secondary air injection does not significantly reduce the total number of particles
411 generated by biomass combustion, but instead shifts the PM size distribution towards smaller,
412 less massive particles.^{20,21,55,56} As the secondary flow rate increases from 7.2 to 12 SLPM, Figure
413 4 shows that the total number of particles emitted from 5 to 2500 nm remains relatively steady,
414 ranging from 5.5×10^{14} to 6.9×10^{14} particles/kWd. Total PM_{2.5} volume, on the other hand,

415 decreases over the range of secondary flow rates presented, as particle size diminishes. Given
 416 that $PM_{2.5}$ density remains nearly constant (Figure B4), the particle volume measurements are
 417 directly proportional to particle mass, and therefore closely mirror the $PM_{2.5}$ mass emission
 418 measurements shown in Figure 2.



419
 420 **Figure 4.** (a) Total $PM_{2.5}$ number and (b) volume emissions from the MOD2 stove over the cold
 421 start (normalized by cooking power), as a function of particle diameter and secondary flow rate
 422 through air injection Pattern 2. (c) Portion of the total number, and (d) volume of particles
 423 emitted in each particle diameter range: 5 to 20 nm, 20 to 100 nm, and 100 to 2500 nm. Each bar
 424 represents the mean of replicate test data collected for each stove configuration. Confidence
 425 intervals are omitted here for clarity, and instead provided in Figure B5.

426 Figure 4 shows that secondary air injection inhibits particle growth, but does not
427 significantly reduce particle formation. Particles form either through nucleation, as volatile
428 organic and inorganic compounds emitted during wood pyrolysis cool in the exhaust, or through
429 soot (BC) generation in the flame.^{15,39,43,57} Typically, these primary particles grow through
430 agglomeration and condensation of volatile compounds. Figure 2 shows that CO and PM_{2.5} mass
431 reductions closely mirror one another as secondary flow rate increases, likely because CO and
432 many-PM forming volatile organic compounds (e.g. PAH) oxidize under similar conditions.^{41,42,58}
433 The portion of PM in the nucleation mode (5 to 20 nm) increases from 20 to 60% as secondary
434 air flow through Pattern 2 increases, likely because particles no longer grow by condensation as
435 volatile organic gas emissions diminish. While number emissions of these small particles
436 increase markedly, they account for less than 2% of the total PM volume, and therefore have
437 little effect on the total mass emitted. Figure B9 provides the size distribution of particle number
438 emissions, and shows a distinct peak at a particle diameter of ~12 nm that increases with
439 secondary flow rate.

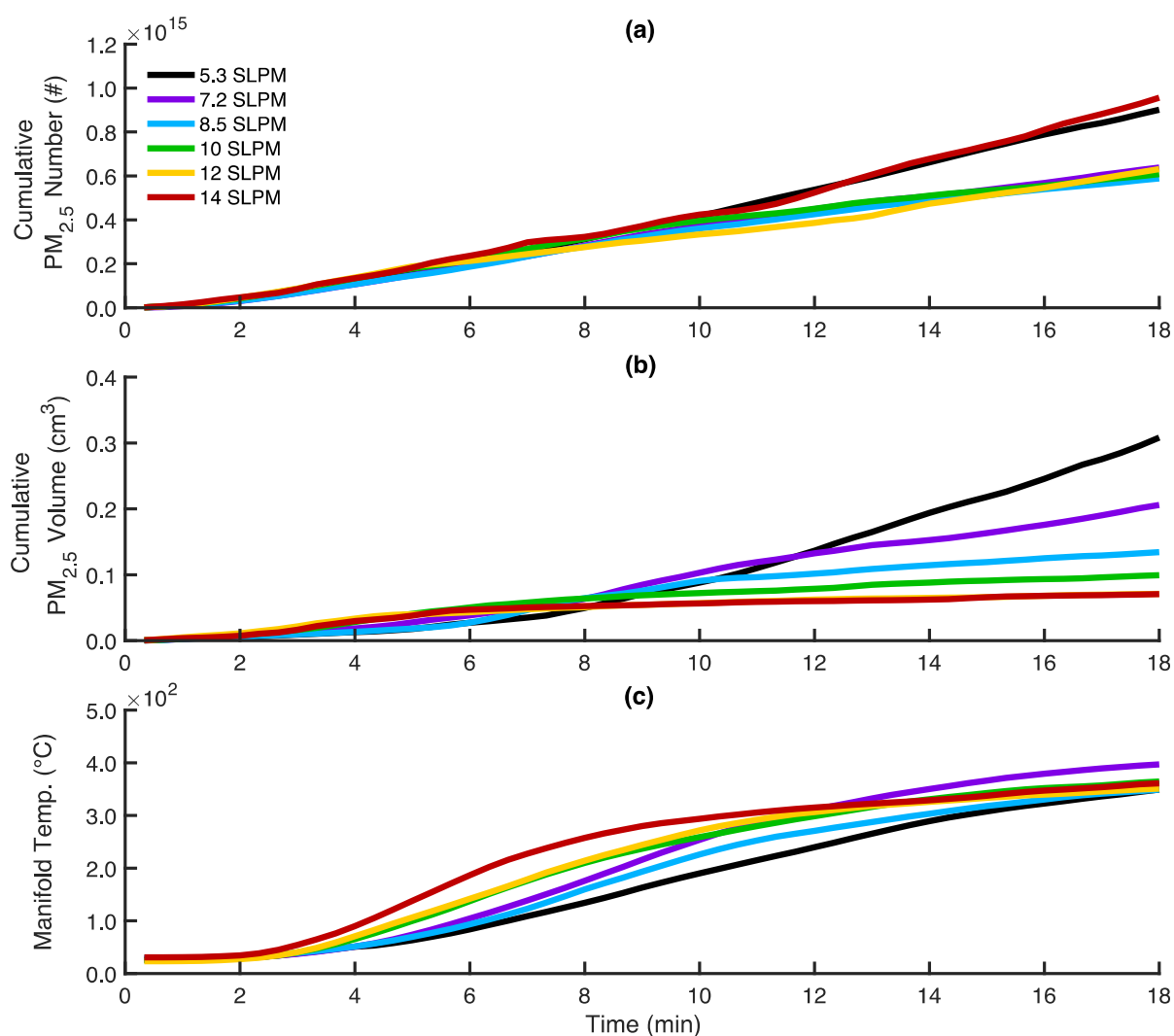
440 In the absence of volatile organic gases in the exhaust, inorganic and BC particles
441 generally grow to sizes <100 nm through agglomeration.^{38,42,44,59} Figure 4 shows that the fraction
442 of total particle number emissions in the UFP range (5 to 100 nm) grows from 80 to 97% as
443 secondary flow increases, and accounts for 20 to 40% of the PM volume generated. As the size
444 distribution shifts towards smaller particles, the fraction of particles in the accumulation mode
445 (100 to 2500 nm) correspondingly decreases from 20 to 3% over the parametric range presented,
446 but still accounts for most (60 to 80%) of the emitted volume. Particles in the accumulation
447 mode form as some growth pathways persist, such the condensation of gases in cool regions of
448 the exhaust flow or agglomeration of particles under turbulent mixing conditions. Throughout the

449 parametric range, nearly all (>> 99.9%) particles emitted are smaller than 1000 nm (6). Larger
450 particles (>1000 nm) account for 0.2 to 0.7% of the total particle volume, and likely consist of fly
451 ash generated in the fuel bed and entrained in the exhaust flow.³⁹

452 Total particle number emissions are lowest for a secondary flow rate of 10 SLPM (Figure
453 4), suggesting that this configuration may provide the optimal balance of turbulent mixing and
454 high combustion temperatures to inhibit particle formation. However, total PM_{2.5} volume
455 generation continues to decrease at higher flow rates, as particle size diminishes. Furthermore,
456 PM_{2.5} number emissions increases sharply from 12 to 14 SLPM, again indicating that excessive
457 secondary flow in this configuration quenches the combustion zone,¹⁷ thereby promoting more
458 PM nucleation. However, total PM_{2.5} volume changes little, as PM emissions in the accumulation
459 mode remain relatively constant. Together, these trends demonstrate that PM_{2.5} mass emission
460 reductions can be achieved while simultaneously generating more UFPs.

461 When the secondary air flow rate is sufficient, the particle size distribution increasingly
462 shifts towards smaller, less massive particles as the stove, fuel, and exhaust gases warm up
463 during the cold start test.⁶⁰ The injection of hotter secondary air at higher velocities also likely
464 contributes to the shift towards smaller particle emissions, as injection velocity increases
465 proportionally with manifold temperature (Equation A5). When the secondary flow rate setting
466 through Pattern 2 increases, Figure 5 shows that particle volume generation is increasingly
467 attenuated over the first 18 minutes of the cold start test, although the number of emitted particles
468 accumulates steadily for all configurations. The PM_{2.5} number and volume accumulation rates
469 reflect the secondary flow dependence illustrated in Figure 4. Manifold temperatures rise more
470 rapidly at higher flow rate settings (Figure 5(c)), thereby hastening the inhibition of particle
471 growth. For flow rates ≥ 10 SLPM, the count median diameter (CMD) of particle emissions

472 decreases from around 60 nm to 20 nm over the first 18 minutes of the cold start (Figure B10),
473 and so most of the particle volume is emitted during start up. At the optimal secondary flow rate
474 setting of 12 SLPM, half of total volume emissions are emitted within the first ~7 minutes
475 following ignition, representing only ~30% of the total test length (in this configuration, the
476 average time to boil is 24 ± 2 min). Consequently, if further PM mass reductions are sought,
477 methods should be developed to enhance combustion conditions during start up.



478

479 **Figure 5.** (a) Accumulation of PM_{2.5} number and (b) volume emissions from the MOD2 stove
480 over the first 18 minutes of the cold start test. (c) Temperature of secondary air in the MOD2
481 stove manifold over the same period. Each line represents the mean of replicate test
482 measurements collected at each of the six secondary flow settings (using air injection Pattern 2).
483 Confidence intervals are omitted here for clarity, and instead provided in Figures B7 and B8 for
484 all secondary flow rate settings. All data presented is block-averaged on a 20-sec time base.

485 Although volume emissions are attenuated over time, the number of particles continues to
486 accumulate steadily for all configurations, and the CMD is less < 80 nm throughout (Figure
487 B10), well within the ultrafine range that is of particular concern for human health. As a result, it
488 is important that future research efforts investigate methods for inhibiting particle formation
489 entirely, rather than simply limiting particle growth. For example, methods of restricting the fuel
490 bed temperature could be devised to limit the volatilization of inorganic compounds that nucleate
491 into incombustible particles.¹⁵

492

493 **4. Conclusion**

494 While further improvements are needed to reduce UFP emissions, the MOD2 stove
495 generally illustrates that secondary air injection is a practical and effective method for reducing
496 mass emissions of PM_{2.5}, CO, and BC from wood combustion. Crucially, we show that emission
497 reductions are achievable using inexpensive hardware that is currently on the market, and can be
498 driven independently using a TEG or other low-cost power source. Stove performance is highly
499 sensitive to secondary air injection design parameters, and so it is important that new designs be
500 validated and optimized experimentally. The experimental results presented here illustrate

501 important design principles that will help to inform the development of clean, efficient, and
502 practical cookstoves that better mitigate harmful air pollution exposure in the billions of
503 households that depend on solid biomass for their daily cooking needs.

504

505

506 **ACKNOWLEDGMENT**

507 This work was performed at the Lawrence Berkeley National Laboratory, operated by the
508 University of California, under DOE Contract DE-AC02-05CH11231. We gratefully
509 acknowledge support for this work from DOE's Biomass Energy Technologies Office. Author
510 Julien J. Caubel is grateful for support from the National Science Foundation's Graduate
511 Research Fellowship Program.

512 The authors would like to recognize the central contribution of Allen Boltz, Marion
513 Laglaive, Guillaume Charbonnel, Varun Khurana, Maelle Seigle and Anouar Mabrouk, who
514 spent countless hours in the laboratory testing the cookstove and collecting the experimental data
515 upon which this research is founded. We would also like to acknowledge the engineering staff at
516 UC Berkeley and Lawrence Berkeley National Laboratory who fabricated the cookstove
517 hardware: Alex Jordan, Jacob Gallego, Jeffrey Olson, Tim Williams, and Rick Kraft. Finally, we
518 thank Dr. Daniel Wilson for his guidance in post-processing the particle emissions data and Gary
519 Hubbard for developing the software tools to simplify data collection from all of our instruments.

520

521 **DECLARATIONS OF INTEREST**

522 None.

523

524 **ABBREVIATIONS**

525 APS, Aerodynamic Particle Sizer; BC, Black Carbon; CAI, California Analytical Instruments;

526 CO₂, Carbon Dioxide; CO, Carbon Monoxide; FMPS, Fast Mobility Particle Sizer; kWd,

527 kilowatt of thermal power delivered to the cooking pot; LBNL, Lawrence Berkeley National

528 Laboratory; MOD, Modular Air Injection Stove: Version 1; MOD2, Modular Air Injection

529 Stove: Version 2; PAH, Polycyclic Aromatic Hydrocarbon; PM, Particulate Matter; PM_{2.5},

530 Particulate Matter with an aerodynamic diameter $\leq 2.5 \mu\text{m}$; ppmv, parts per million by volume;

531 TEG, Thermoelectric Generator; TSF, Three Stone Fire; UFP, Ultrafine Particle; US EPA,

532 United States Environmental Protection Agency; WBT, Water Boiling Test; WHO, World

533 Health Organization.

534

535

536 **REFERENCES:**

- 537 (1) Bonjour, S.; Adair-Rohani, H.; Wolf, J.; Bruce, N. G.; Mehta, S.; Prüss-Ustün, A.;
538 Lahiff, M.; Rehfuess, E. A.; Mishra, V.; Smith, K. R. Solid Fuel Use for Household
539 Cooking: Country and Regional Estimates for 1980–2010. *Environ. Health Perspect.*
540 **2013**, *121* (7), 784–790.
- 541 (2) Legros, G.; Havet, I.; Bruce, N. G.; Bonjour, S. *The Energy Access Situation in*
542 *Developing Countries*; United Nations Development Programme (UNDP): New York,
543 2009; pp 1–142.
- 544 (3) Bruce, N. G.; Perez-Padilla, R.; Albalak, R. Indoor Air Pollution in Developing
545 Countries: a Major Environmental and Public Health Challenge. *Bulletin of the World*
546 *Health Organization* **2000**, *78* (9), 1078–1092.
- 547 (4) Malla, S.; Timilsina, G. R. *Household Cooking Fuel Choice and Adoption of Improved*
548 *Cookstoves in Developing Countries*; The World Bank, 2014; pp 1–52.
- 549 (5) Edwards, R.; Karnani, S.; Fisher, E. M.; Johnson, M.; Naeher, L.; Smith, K. R.;
550 Morawska, L. *WHO Indoor Air Quality Guidelines: Household Fuel Combustion*; World
551 Health Organization, 2014; pp 1–42.
- 552 (6) Smith, K. R.; Dutta, K.; Chengappa, C.; Gusain, P. P.; Masera, O.; Berrueta, V.;
553 Edwards, R.; Bailis, R.; Shields, K. N. Monitoring and Evaluation of Improved Biomass
554 Cookstove Programs for Indoor Air Quality and Stove Performance: Conclusions From
555 the Household Energy and Health Project. *Energy for Sustainable Development* **2007**, *11*
556 (2), 5–18.
- 557 (7) Chen, C.; Zeger, S.; Breysse, P.; Katz, J.; Checkley, W.; Curriero, F. C.; Tielsch, J. M.

558 Estimating Indoor PM_{2.5} and CO Concentrations in Households in Southern Nepal: the
559 Nepal Cookstove Intervention Trials. *PLoS ONE* **2016**, *11* (7), e0157984–17.

560 (8) Stanaway, J. D.; Afshin, A.; Gakidou, E.; Lim, S. S.; Abate, D.; Abate, K. H.; Abbafati,
561 C.; Abbasi, N.; Abbastabar, H.; Abd-Allah, F.; Abdela, J.; Abdelalim, A.; Abdollahpour,
562 I.; Abdulkader, R. S.; Abebe, M.; Abebe, Z.; Abera, S. F.; Abil, O. Z.; Abraha, H. N.;
563 Abrham, A. R.; Abu-Raddad, L. J.; Abu-Rmeileh, N. M.; Accrombessi, M. M. K.;
564 Acharya, D.; Acharya, P.; Adamu, A. A.; Adane, A. A.; Adebayo, O. M.; Adedoyin, R.
565 A.; Adekanmbi, V.; Ademi, Z.; Adetokunboh, O. O.; Adib, M. G.; Admasie, A.; Adsuar,
566 J. C.; Afanvi, K. A.; Afarideh, M.; Agarwal, G.; Aggarwal, A.; Aghayan, S. A.;
567 Agrawal, A.; Agrawal, S.; Ahmadi, A.; Ahmadi, M.; Ahmadi, H.; Ahmed, M. B.;
568 Aichour, A. N.; Aichour, I.; Aichour, M. T. E.; Akbari, M. E.; Akinyemiju, T.; Akseer,
569 N.; Al-Aly, Z.; Al-Eyadhy, A.; Al-Mekhlafi, H. M.; Alahdab, F.; Alam, K.; Alam, S.;
570 Alam, T.; Alashi, A.; Alavian, S. M.; Alene, K. A.; Ali, K.; Ali, S. M.; Alijanzadeh, M.;
571 Alizadeh-Navaei, R.; Aljunid, S. M.; Alkerwi, A.; Alla, F. O.; Alsharif, U.; Altirkawi,
572 K.; Alvis-Guzman, N.; Amare, A. T.; Ammar, W.; Anber, N. H.; Anderson, J. A.;
573 Andrei, C. L.; Androudi, S.; Animut, M. D.; Anjomshoa, M.; Ansha, M. G.; Ant³, J.
574 M.; Antonio, C. A. T.; Anwari, P.; Appiah, L. T.; Appiah, S. C. Y.; Arabloo, J.; Aremu,
575 O.; v, J. A. R.; Artaman, Al; Aryal, K. K.; Asayesh, H.; Ataro, Z.; Ausloos, M.;
576 Avokpaho, E. F. G. A.; Awasthi, A.; Quintanilla, B. P. A.; Ayer, R.; Ayuk, T. B.;
577 Azzopardi, P. S.; Babazadeh, A.; Badali, H.; Badawi, A.; Balakrishnan, K.; Bali, A. G.;
578 Ball, K.; Ballew, S. H.; Banach, M.; Banoub, J. A. M.; Barac, A.; Barker-Collo, S. L.;
579 rnighausen, T. W. B.; Barrero, L. H.; Basu, S.; Baune, B. T.; Bazargan-Hejazi, S.; Bedi,

580 N.; Beghi, E.; Behzadifar, M.; Behzadifar, M.; jot, Y. B.; Bekele, B. B.; Bekru, E. T.;

581 Belay, E.; Belay, Y. A.; Bell, M. L.; Bello, A. K.; Bennett, D. A.; Bensenor, I. M.;

582 Bergeron, G.; Berhane, A.; Bernabe, E.; Bernstein, R. S.; Beuran, M.; Beyranvand, T.;

583 Bhala, N.; Bhalla, A.; Bhattarai, S.; Bhutta, Z. A.; Biadgo, B.; Bijani, A.; Bikbov, B.;

584 Ver Bilano; Bililign, N.; Bin Sayeed, M. S.; Bisanzio, D.; Biswas, T.; rge, T. B.;

585 Blacker, B. F.; Bleyer, A.; Borschmann, R.; Bou-Orm, I. R.; Boufous, S.; Bourne, R.;

586 Brady, O. J.; Brauer, M.; Brazinova, A.; Breitborde, N. J. K.; Brenner, H.; Briko, A. N.;

587 Britton, G.; Brugha, T.; Buchbinder, R.; Burnett, R. T.; Busse, R.; Butt, Z. A.; Cahill, L.

588 E.; Cahuana-Hurtado, L.; Campos-Nonato, I. R.; rdenas, R. C.; Carreras, G.; Carrero, J.

589 J.; Carvalho, F. L.; eda-Orjuela, C. A. C.; Rivas, J. C.; Castro, F.; pez, F. N. C. L.;

590 Causey, K.; Cercy, K. M.; Cerin, E.; Chaiah, Y.; Chang, H.-Y.; Chang, J.-C.; Chang, K.-

591 L.; Charlson, F. J.; Chattopadhyay, A.; Chattu, V. K.; Chee, M. L.; Cheng, C.-Y.; Chew,

592 A.; Chiang, P. P.-C.; Chimed-Ochir, O.; Chin, K. L.; Chitheer, A.; Choi, J.-Y. J.;

593 Chowdhury, R.; Christensen, H.; Christopher, D. J.; Chung, S.-C.; Cicuttini, F. M.;

594 Cirillo, M.; Cohen, A. J.; Collado-Mateo, D.; Cooper, C.; Cooper, O. R.; Coresh, J.;

595 Cornaby, L.; Cortesi, P. A.; Cortinovis, M.; Costa, M.; Cousin, E.; Criqui, M. H.;

596 Cromwell, E. A.; Cundiff, D. K.; Daba, A. K.; Dachew, B. A.; Dadi, A. F.; Damasceno,

597 A. A. M.; Dandona, L.; Dandona, R.; Darby, S. C.; Dargan, P. I.; Daryani, A.; Gupta,

598 Das, R.; Neves, das, J.; Dasa, T. T.; Dash, A. P.; Davitoiu, D. V.; Davletov, K.; la Cruz-

599 GÃ ngora, De, V.; La Hoz, De, F. P.; De Leo, D.; De Neve, J.-W.; Degenhardt, L.;

600 Deiparine, S.; Dellavalle, R. P.; Demoz, G. T.; rrez, E. D.-G.; Deribe, K.; Dervenis, N.;

601 Deshpande, A.; Jarlais, Des, D. C.; Dessie, G. A.; Deveber, G. A.; Dey, S.;

602 Dharmaratne, S. D.; Dhimal, M.; Dinberu, M. T.; Ding, E. L.; Diro, H. D.; Djalalinia, S.;

603 Do, H. P.; Dokova, K.; Doku, D. T.; Doyle, K. E.; Driscoll, T. R.; Dubey, M.;

604 Dubljanin, E.; Duken, E. E.; Duncan, B. B.; Duraes, A. R.; Ebert, N.; Ebrahimi, H.;

605 Ebrahimpour, S.; Edvardsson, D.; Effiong, A.; Eggen, A. E.; Bcheraoui, El, C.; El-

606 Khatib, Z.; Elyazar, I. R.; Enayati, A.; Endries, A. Y.; Er, B.; Erskine, H. E.;

607 Eskandarieh, S.; Esteghamati, A.; Estep, K.; Fakhim, H.; Faramarzi, M.; Fareed, M.;

608 Farid, T. A.; Farinha, C. S. E. S.; Farioli, A.; Faro, A.; Farvid, M. S.; Farzaei, M. H.;

609 Fatima, B.; Fay, K. A.; Fazaeli, A. A.; Feigin, V. L.; Feigl, A. B.; Fereshtehnejad, S.-M.;

610 Fernandes, E.; Fernandes, J. C.; Ferrara, G.; Ferrari, A. J.; Ferreira, M. L.; Filip, I.;

611 Finger, J. D.; Fischer, F.; Foigt, N. A.; Foreman, K. J.; Fukumoto, T.; Fullman, N.;

612 FÅ¼rst, T.; Furtado, J. O. M.; Futran, N. D.; Gall, S.; Gallus, S.; Gamkrelidze, A.;

613 Ganji, M.; Garcia-Basteiro, A. L.; Gardner, W. M.; Gebre, A. K.; Gebremedhin, A. T.;

614 Gebremichael, T. G.; Gelano, T. F.; Geleijnse, J. M.; Geramo, Y. C. D.; Gething, P. W.;

615 Gezae, K. E.; Ghadimi, R.; Ghadiri, K.; Falavarjani, K. G.; Ghasemi-Kasman, M.;

616 Ghimire, M.; Ghosh, R.; Ghoshal, A. G.; Giampaoli, S.; Gill, P. S.; Gill, T. K.; Gillum,

617 R. F.; Ginawi, I. A.; Giussani, G.; Gnedovskaya, E. V.; Godwin, W. W.; Goli, S.; s, H.

618 G. M.-D.; Gona, P. N.; Gopalani, S. V.; Goulart, A. C.; Grada, A.; Grams, M. E.;

619 Grosso, G.; Gugnani, H. C.; Guo, Y.; Gupta, R.; Gupta, R.; Gupta, T.; rrez, R. A. G.;

620 rrez-Torres, D. S. G.; Haagsma, J. A.; Habtewold, T. D.; Hachinski, V.; Hafezi-Nejad,

621 N.; Hagos, T. B.; Hailegiyorgis, T. T.; Hailu, G. B.; Haj-Mirzaian, A.; Haj-Mirzaian, A.;

622 Hamadeh, R. R.; Hamidi, S.; Handal, A. J.; Hankey, G. J.; Hao, Y.; Harb, H. L.;

623 Harikrishnan, S.; Haro, J. M.; Hassankhani, H.; Hassen, H. Y.; Havmoeller, R.; Hawley,

624 C. N.; Hay, S. I.; Hedayatizadeh-Omran, A.; Heibati, B.; Heidari, B.; Heidari, M.;

625 Hendrie, D.; Henok, A.; Heredia-Pi, I.; Herteliu, C.; Heydarpour, F.; Heydarpour, S.;

626 Hibstu, D. T.; Higazi, T. B.; Hilawe, E. H.; Hoek, H. W.; Hoffman, H. J.; Hole, M. K.;
627 Rad, E. H.; Hoogar, P.; Hosgood, H. D.; Hosseini, S. M.; Hosseinzadeh, M.; Hostiuc,
628 M.; Hostiuc, S.; Hoy, D. G.; Hsairi, M.; Hsiao, T.; Hu, G.; Hu, H.; Huang, J. J.; Hussen,
629 M. A.; Huynh, C. K.; Iburg, K. M.; Ikeda, N.; Ilesanmi, O. S.; Iqbal, U.; Irvani, S. S. N.;
630 Irvine, C. M. S.; Islam, S. M. S.; Islami, F.; Jackson, M. D.; Jacobsen, K. H.; Jahangiry,
631 L.; Jahanmehr, N.; Jain, S. K.; Jakovljevic, M.; James, S. L.; Jassal, S. K.; Jayatilleke, A.
632 U.; Jeemon, P.; Jha, R. P.; Jha, V.; Ji, J. S.; Jonas, J. B.; Jonnagaddala, J.; Shushtari, Z.
633 J.; Joshi, A.; Jozwiak, J. J.; Järvisson, M.; Kabir, Z.; Kahsay, A.; Kalani, R.; Kanchan,
634 T.; Kant, S.; Kar, C.; Karami, M.; Matin, B. K.; Karch, A.; Karema, C.; Karimi, N.;
635 Karimi, S. M.; Kasaeian, A.; Kassa, D. H.; Kassa, G. M.; Kassa, T. D.; Kassebaum, N.
636 J.; Katikireddi, S. V.; Kaul, A.; Kawakami, N.; Kazemi, Z.; Karyani, A. K.; Kefale, A.
637 T.; Keiyoro, P. N.; Kemp, G. R.; Kengne, A. P.; Keren, A.; Kesavachandran, C. N.;
638 Khader, Y. S.; Khafaei, B.; Khafaie, M. A.; Khajavi, A.; Khalid, N.; Khalil, I. A.; Khan,
639 G.; Khan, M. S.; Khan, M. A.; Khang, Y.-H.; Khater, M. M.; Khazaei, M.; Khazaie, H.;
640 Khoja, A. T.; Khosravi, A.; Khosravi, M. H.; Kiadaliri, A. A.; Kiirithio, D. N.; Kim, C.-
641 I.; Kim, D.; Kim, Y.-E.; Kim, Y. J.; Kimokoti, R. W.; Kinfu, Y.; Kisa, A.; Kissimova-
642 Skarbek, K.; Ki, M. K.; Knibbs, L. D.; Knudsen, A. K. S.; Kochhar, S.; Kokubo, Y.;
643 Kolola, T.; Kopec, J. A.; Kosen, S.; Koul, P. A.; Koyanagi, A.; Kravchenko, M. A.;
644 Krishan, K.; Krohn, K. J.; Kromhout, H.; Defo, B. K.; Bicer, B. K.; Kumar, G. A.;
645 Kumar, M.; Kuzin, I.; Kyu, H. H.; Lachat, C.; Lad, D. P.; Lad, S. D.; Lafranconi, A.;
646 Laloo, R.; Lallukka, T.; Lami, F. H.; Lang, J. J.; Van C Lansingh; Larson, S. L.; Latifi,
647 A.; Lazarus, J. V.; Lee, P. H.; Leigh, J.; Leili, M.; Leshargie, C. T.; Leung, J.; Levi, M.;
648 Lewycka, S.; Li, S.; Li, Y.; Liang, J.; Liang, X.; Liao, Y.; Liben, M. L.; Lim, L.-L.;

649 Linn, S.; Liu, S.; Lodha, R.; Logroscino, G.; Lopez, A. D.; Lorkowski, S.; Lotufo, P. A.;
650 Lozano, R.; Lucas, T. C. D.; Lunevicius, R.; Ma, S.; Macarayan, E. R. K.; Machado, Ã.
651 S. E.; Madotto, F.; Mai, H. T.; Majdan, M.; Majdzadeh, R.; Majeed, A.; Malekzadeh, R.;
652 Malta, D. C.; Mamun, A. A.; Manda, A.-L.; Manguerra, H.; Mansournia, M. A.;
653 Mantovani, L. G.; Maravilla, J. C.; Marcenes, W.; Marks, A.; Martin, R. V.; Martins, S.
654 C. O.; Martins-Melo, F. R. N.; rz, W. M.; Marzan, M. B.; Massenbunrg, B. B.; Mathur,
655 M. R.; Mathur, P.; Matsushita, K.; Maulik, P. K.; Mazidi, M.; McAlinden, C.; McGrath,
656 J. J.; McKee, M.; Mehrotra, R.; Mehta, K. M.; Mehta, V.; Meier, T.; Mekonnen, F. A.;
657 Melaku, Y. A.; Melese, A.; Melku, M.; Memiah, P. T. N.; Memish, Z. A.; Mendoza, W.;
658 Mengistu, D. T.; Mensah, G. A.; Mensink, G. B. M.; Mereta, S. T.; Meretoja, A.;
659 Meretoja, T. J.; Mestrovic, T.; Mezgebe, H. B.; Miazgowski, B.; Miazgowski, T.;
660 Milllear, A. I.; Miller, T. R.; Miller-Petrie, M. K.; Mini, G. K.; Mirarefin, M.; Mirica, A.;
661 Mirrakhimov, E. M.; Misganaw, A. T.; Mitiku, H.; Moazen, B.; Mohajer, B.;
662 Mohammad, K. A.; Mohammadi, M.; Mohammadifard, N.; Mohammadnia-Afrouzi, M.;
663 Mohammed, S.; Mohebi, F.; Mokdad, A. H.; Molokhia, M.; Momeniha, F.; Monasta, L.;
664 Moodley, Y.; Moradi, G.; Moradi-Lakeh, M.; Moradinazar, M.; Moraga, P.; Morawska,
665 L.; Morgado-Da-Costa, J.; Morrison, S. D.; Moschos, M. M.; Mouodi, S.; Mousavi, S.
666 M.; Mozaffarian, D.; Mruts, K. B.; Muche, A. A.; Muchie, K. F.; Mueller, U. O.;
667 Muhammed, O. S.; Mukhopadhyay, S.; Muller, K.; Musa, K. I.; Mustafa, G.; Nabhan, A.
668 F.; Naghavi, M.; Naheed, A.; Nahvijou, A.; Naik, G.; Naik, N.; Najafi, F.; Nangia, V.;
669 Nansseu, J. R.; Nascimento, B. R.; Neal, B.; Neamati, N.; Negoj, I.; Negoj, R. I.;
670 Neupane, S.; Newton, C. R. J.; Ngunjiri, J. W.; Nguyen, A. Q.; Nguyen, G.; Nguyen, H.
671 T.; Nguyen, H. L. T.; Nguyen, H. T.; Nguyen, M.; Nguyen, N. B.; Nichols, E.; Nie, J.;

672 Ningrum, D. N. A.; Nirayo, Y. L.; Nishi, N.; Nixon, M. R.; Nojomi, M.; Nomura, S.;

673 Norheim, O. F.; Noroozi, M.; Norrving, B.; Noubiap, J. J.; Nouri, H. R.; Shiadeh, M. N.;

674 Nowroozi, M. R.; Nsoesie, E. O.; Nyasulu, P. S.; Obermeyer, C. M.; Odell, C. M.;

675 Ofori-Asenso, R.; Ogbo, F. A.; Oh, I.-H.; Oladimeji, O.; Olagunju, A. T.; Olagunju, T.

676 O.; Olivares, P. R.; Olsen, H. E.; Olusanya, B. O.; Olusanya, J. O.; Ong, K. L.; Ong, S.

677 K.; Oren, E.; Orpana, H. M.; Ortiz, A.; Ota, E.; Otstavnov, S. S.; verland, S. Ã.;

678 Owolabi, M. O.; A, M. P.; Pacella, R.; Pakhare, A. P.; Pakpour, A. H.; Pana, A.; Panda-

679 Jonas, S.; Park, E.-K.; Parry, C. D. H.; Parsian, H.; Patel, S.; Pati, S.; Patil, S. T.; Patle,

680 A.; Patton, G. C.; Paudel, D.; Paulson, K. R.; Ballesteros, W. C. P.; Pearce, N.; Pereira,

681 A.; Pereira, D. M.; Perico, N.; Pesudovs, K.; Petzold, M.; Pham, H. Q.; Phillips, M. R.;

682 Pillay, J. D.; Piradov, M. A.; Pirsaeheb, M.; Pischon, T.; Pishgar, F.; Plana-Ripoll, O.;

683 Plass, D.; Polinder, S.; Polkinghorne, K. R.; Postma, M. J.; Poulton, R.; Pourshams, A.;

684 Poustchi, H.; Prabhakaran, D.; Prakash, S.; Prasad, N.; Purcell, C. A.; Purwar, M. B.;

685 Qorbani, M.; Radfar, A.; Rafay, A.; Rafiei, A.; Rahim, F.; Rahimi, Z.; Rahimi-

686 Movaghar, A.; Rahimi-Movaghar, V.; Rahman, M.; Rahman, M. H. U.; Rahman, M. A.;

687 Rai, R. K.; Rajati, F.; Rajsic, S.; Raju, S. B.; Ram, U.; Ranabhat, C. L.; Ranjan, P.; Rath,

688 G. K.; Rawaf, D. L.; Rawaf, S.; Reddy, K. S.; Rehm, C. D.; Rehm, J.; Reiner, R. C., Jr;

689 Reitsma, M. B.; Remuzzi, G.; Renzaho, A. M. N.; Resnikoff, S.; Reynales-Shigematsu,

690 L. M.; Rezaei, S.; Ribeiro, A. L. P.; Rivera, J. A.; Roba, K. T.; rez, S. R. G.-R.; Roever,

691 L.; n, Y. R.; Ronfani, L.; Roshandel, G.; Rostami, A.; Roth, G. A.; Rothenbacher, D.;

692 Roy, A.; Rubagotti, E.; Rushton, L.; Sabanayagam, C.; Sachdev, P. S.; Saddik, B.;

693 Sadeghi, E.; Moghaddam, S. S.; Safari, H.; Safari, Y.; Safari-Faramani, R.; Safdarian,

694 M.; Safi, S.; Safiri, S.; Sagar, R.; Sahebkar, A.; Sahraian, M. A.; Sajadi, H. S.; Salam,

695 N.; Salamati, P.; Saleem, Z.; Salimi, Y.; Salimzadeh, H.; Salomon, J. A.; Salvi, D. D.;

696 Salz, I.; Samy, A. M.; Sanabria, J.; o, M. D. S.-N.; nchez-Pimienta, T. G. S.; Sanders, T.;

697 Sang, Y.; Santomauro, D. F.; Santos, I. S.; Santos, J. O. V.; Milicevic, M. M. S.; Jose, B.

698 P. S.; Sardana, M.; Sarker, A. R.; rez, R. S.-S.; Sarrafzadegan, N.; Sartorius, B.; Sarvi,

699 S.; Sathian, B.; Satpathy, M.; Sawant, A. R.; Sawhney, M.; Saylan, M.; Sayyah, M.;

700 Schaeffner, E.; Schmidt, M. I.; Schneider, I. J. C.; Ben SchÃ ttker; Schutte, A. E.;

701 Schwebel, D. C.; Schwendicke, F.; Scott, J. G.; Seedat, S.; Sekerija, M.; Sepanlou, S. G.;

702 Serre, M. L.; n-Mori, E. S.; Seyedmousavi, S.; Shabaninejad, H.; Shaddick, G.;

703 Shafieesabet, A.; Shahbazi, M.; Shaheen, A. A.; Shaikh, M. A.; Levy, T. S.; Shams-

704 Beyranvand, M.; Shamsi, M.; Sharafi, H.; Sharafi, K.; Sharif, M.; Sharif-Alhoseini, M.;

705 Sharifi, H.; Sharma, J.; Sharma, M.; Sharma, R.; She, J.; Sheikh, A.; Shi, P.; Shibuya,

706 K.; Shiferaw, M. S.; Shigematsu, M.; Shin, M.-J.; Shiri, R.; Shirkoohi, R.; Shiue, I.;

707 Shokraneh, F.; Shoman, H.; Shrime, M. G.; Shupler, M. S.; Si, S.; Siabani, S.; Sibai, A.

708 M.; Siddiqi, T. J.; Sigfusdottir, I. D.; Sigurvinsdottir, R.; Silva, D. A. S.; Silva, J. O. P.;

709 Silveira, D. G. A.; Singh, J. A.; Singh, N. P.; Singh, V.; Sinha, D. N.; Skiadaresi, E.;

710 Skirbekk, V.; Smith, D. L.; Smith, M.; Sobaih, B. H.; Sobhani, S.; Somayaji, R.; Soofi,

711 M.; Sorensen, R. J. D.; Soriano, J. B.; Soyiri, I. N.; Spinelli, A.; Sposato, L. A.;

712 Sreeramareddy, C. T.; Srinivasan, V.; Starodubov, V. I.; Steckling, N.; Stein, D. J.;

713 Stein, M. B.; Stevanovic, G.; Stockfelt, L.; Stokes, M. A.; Sturua, L.; Subart, M. L.;

714 Sudaryanto, A.; Sufiyan, M. B.; Sulo, G.; Sunguya, B. F.; Sur, P. J.; Sykes, B. L.;

715 Szoeki, C. E. I.; s-Seisdodos, R. T.; Tabuchi, T.; Tadakamadla, S. K.; Takahashi, K.;

716 Tandon, N.; Tassew, S. G.; Tavakkoli, M.; Taveira, N.; Tehrani-Banihashemi, A.;

717 Tekalign, T. G.; Tekelemedhin, S. W.; Tekle, M. G.; Temesgen, H.; Temsah, M.-H.;

718 Temsah, O.; Terkawi, A. S.; Tessema, B.; Teweldemedhin, M.; Thankappan, K. R.;

719 Theis, A.; Thirunavukkarasu, S.; Thomas, H. J.; Thomas, M. L.; Thomas, N.; Thurston,

720 G. D.; Tilahun, B.; Tillmann, T.; To, Q. G.; Tobollik, M.; Tonelli, M.; Topor-Madry, R.;

721 Torre, A. E.; s, M. T.-G.; Touvier, M.; Tovani-Palone, M. R.; Towbin, J. A.; Tran, B. X.;

722 Tran, K. B.; Truelsen, T. C.; Truong, N. T.; Tsadik, A. G.; Car, L. T.; Tuzcu, E. M.;

723 Tymeson, H. D.; Tyrovolas, S.; Ukwaja, K. N.; Ullah, I.; Updike, R. L.; Usman, M. S.;

724 Uthman, O. A.; Vaduganathan, M.; Vaezi, A.; Valdez, P. R.; van Donkelaar, A.;

725 Varavikova, E.; Varughese, S.; Vasankari, T. J.; Venkateswaran, V.;

726 Venketasubramanian, N.; Villafaina, S.; Violante, F. S.; Vladimirov, S. K.; Vlassov, V.;

727 Vollset, S. E.; Vos, T.; Vosoughi, K.; Vu, G. T.; Vujcic, I. S.; Wagnew, F. S.; Waheed,

728 Y.; Waller, S. G.; Walson, J. L.; Wang, Y.; Wang, Y.; Wang, Y.-P.; Weiderpass, E.;

729 Weintraub, R. G.; Weldegebreal, F.; Werdecker, A.; Werkneh, A. A.; West, J. J.;

730 Westerman, R.; Whiteford, H. A.; Widecka, J.; Wijeratne, T.; Winkler, A. S.; Wiyeh, A.

731 B.; Wiysonge, C. S.; Wolfe, C. D. A.; Wong, T. Y.; Wu, S.; Xavier, D.; Xu, G.; Yadgir,

732 S.; Yadollahpour, A.; Jabbari, S. H. Y.; Yamada, T.; Yan, L. L.; Yano, Y.; Yaseri, M.;

733 Yasin, Y. J.; Yeshaneh, A.; Yimer, E. M.; Yip, P.; Yisma, E.; Yonemoto, N.; Yoon, S.-

734 J.; Yotebieng, M.; Younis, M. Z.; Yousefifard, M.; Yu, C.; Zaidi, Z.; Bin Zaman, S.;

735 Zamani, M.; Zavala-Arciniega, L.; Zhang, A. L.; Zhang, H.; Zhang, K.; Zhou, M.;

736 Zimsen, S. R. M.; Zodpey, S.; Murray, C. J. L.; Collaborators, G. 2. R. F. Global,

737 Regional, and National Comparative Risk Assessment of 84 Behavioural, Environmental

738 and Occupational, and Metabolic Risks or Clusters of Risks for 195 Countries and

739 Territories, 1990-2017: a Systematic Analysis for the Global Burden of Disease Study

- 740 2017. *The Lancet* **2018**, 392 (10159), 1923–1994.
- 741 (9) Foell, W.; Pachauri, S.; Spreng, D.; Zerriffi, H. Household Cooking Fuels and
742 Technologies in Developing Economies. *Energy Policy* **2011**, 39 (12), 7487–7496.
- 743 (10) Jetter, J.; Zhao, Y.; Smith, K. R.; Khan, B.; Yelverton, T.; DeCarlo, P.; Hays, M. D.
744 Pollutant Emissions and Energy Efficiency Under Controlled Conditions for Household
745 Biomass Cookstoves and Implications for Metrics Useful in Setting International Test
746 Standards. *Environ. Sci. Technol.* **2012**, 46 (19), 10827–10834.
- 747 (11) Jetter, J.; Ebersviller, S. *Test Report: BioLite HomeStove with Wood Fuel*; U.S.
748 Environmental Protection Agency, 2015; pp 1–33.
- 749 (12) Delapena, S.; Garland, C.; Jagoe, K.; Okada, E.; Ouk, S.; Pennise, D.; Pillarisetti, A.;
750 Steele, J. *Quantifying the Health Impacts of ACE-1 Biomass and Biogas Stoves in*
751 *Cambodia*; Berkeley Air Monitoring Group, 2015; pp 1–52.
- 752 (13) Still, D.; Bentson, S.; Li, H. Results of Laboratory Testing of 15 Cookstove Designs in
753 Accordance with the ISO/IWA Tiers of Performance. *EcoHealth* **2015**, 12, 12–24.
- 754 (14) Sutar, K. B.; Kohli, S.; Ravi, M. R.; Ray, A. Biomass Cookstoves: a Review of
755 Technical Aspects. *Renewable and Sustainable Energy Reviews* **2015**, 41, 1128–1166.
- 756 (15) Lamberg, H.; Sippula, O.; Tissari, J.; Jokiniemi, J. Effects of Air Staging and Load on
757 Fine-Particle and Gaseous Emissions From a Small-Scale Pellet Boiler. *Energy Fuels*
758 **2011**, 25 (11), 4952–4960.
- 759 (16) Lyngfelt, A.; Leckner, B. Combustion of Wood-Chips in Circulating Fluidized Bed
760 Boilers — NO and CO Emissions as Functions of Temperature and Air-Staging. *Fuel*
761 **1999**, 78, 1065–1072.

- 762 (17) Nuutinen, K.; Jokiniemi, J.; Sippula, O.; Lamberg, H.; Sutinen, J.; Horttanainen, P.;
763 Tissari, J. Effect of Air Staging on Fine Particle, Dust and Gaseous Emissions From
764 Masonry Heaters. *Biomass and Bioenergy* **2014**, *67*, 167–178.
- 765 (18) Okasha, F. Staged Combustion of Rice Straw in a Fluidized Bed. *Experimental Thermal
766 and Fluid Science* **2007**, *32* (1), 52–59.
- 767 (19) Wiinikka, H.; Gebart, R. Critical Parameters for Particle Emissions in Small-Scale
768 Fixed-Bed Combustion of Wood Pellets. *Energy Fuels* **2004**, *18* (4), 897–907.
- 769 (20) Caubel, J. J.; Rapp, V. H.; Chen, S. S.; Gadgil, A. J. Optimization of Secondary Air
770 Injection in a Wood-Burning Cookstove: an Experimental Study. *Environ. Sci. Technol.*
771 **2018**, *52* (7), 4449–4456.
- 772 (21) Rapp, V. H.; Caubel, J. J.; Wilson, D. L.; Gadgil, A. J. Reducing Ultrafine Particle
773 Emissions Using Air Injection in Wood-Burning Cookstoves. *Environ. Sci. Technol.*
774 **2016**, *50* (15), 8368–8374.
- 775 (22) Pettersson, E.; Lindmark, F.; Öhman, M.; Nordin, A.; Westerholm, R.; Boman, C.
776 Design Changes in a Fixed-Bed Pellet Combustion Device: Effects of Temperature and
777 Residence Time on Emission Performance. *Energy Fuels* **2010**, *24* (2), 1333–1340.
- 778 (23) Tryner, J.; Tillotson, J. W.; Baumgardner, M. E.; Mohr, J. T.; DeFoort, M. W.;
779 Marchese, A. J. The Effects of Air Flow Rates, Secondary Air Inlet Geometry, Fuel
780 Type, and Operating Mode on the Performance of Gasifier Cookstoves. *Environ. Sci.*
781 *Technol.* **2016**, *50* (17), 9754–9763.
- 782 (24) Nussbaumer, T. Combustion and Co-Combustion of Biomass: Fundamentals,
783 Technologies, and Primary Measures for Emission Reduction †. *Energy Fuels* **2003**, *17*

- 784 (6), 1510–1521.
- 785 (25) Vicente, E. D.; Alves, C. A. An Overview of Particulate Emissions From Residential
786 Biomass Combustion. *Atmospheric Research* **2018**, *199*, 159–185.
- 787 (26) Soneja, S. I.; Tielsch, J. M.; Curriero, F. C.; Zaitchik, B.; Khatry, S. K.; Yan, B.;
788 Chillrud, S. N.; Breyse, P. N. Determining Particulate Matter and Black Carbon
789 Exfiltration Estimates for Traditional Cookstove Use in Rural Nepalese Village
790 Households. *Environ. Sci. Technol.* **2015**, *49* (9), 5555–5562.
- 791 (27) Lienhard, J. H., V; Lienhard, J. H., IV. Velocity Coefficients for Free Jets From Sharp-
792 Edged Orifices. *Journal of Fluids Engineering* **1984**, *106* (13), 13–17.
- 793 (28) Cushman-Roisin, B. Turbulent Jets. In *Environmental Fluid Mechanics*; New York,
794 2014; pp 1–9.
- 795 (29) *The Water Boiling Test*, 4 ed.; Global Alliance for Clean Cookstoves, 2014; pp 1–89.
- 796 (30) Bilsback, K. R.; Eilenberg, S. R.; Good, N.; Heck, L.; Johnson, M.; Kodros, J. K.;
797 Lipsky, E. M.; L'Orange, C.; Pierce, J. R.; Robinson, A. L.; Subramanian, R.; Tryner, J.;
798 Wilson, A.; Volckens, J. The Firepower Sweep Test: a Novel Approach to Cookstove
799 Laboratory Testing. *Indoor Air* **2018**, *28* (6), 936–949.
- 800 (31) Wang, Y.; Sohn, M. D.; Wang, Y.; Lask, K. M.; Kirchstetter, T. W.; Gadgil, A. J. How
801 Many Replicate Tests Are Needed to Test Cookstove Performance and Emissions? —
802 Three Is Not Always Adequate. *Energy for Sustainable Development* **2014**, *20*, 21–29.
- 803 (32) Taylor, J. R. *An Introduction to Error Analysis: the Study of Uncertainties in Physical*
804 *Measurements*; University Science Books: Sausalito, CA, 1997; pp 1–1.
- 805 (33) Bäfver, L. S.; Leckner, B.; Tullin, C.; Berntsen, M. Particle Emissions From Pellets

- 806 Stoves and Modern and Old-Type Wood Stoves. *Biomass and Bioenergy* **2011**, 35 (8),
807 3648–3655.
- 808 (34) Houshfar, E.; Skreiberg, Ø.; Løvås, T.; Todorović, D.; Sørum, L. Effect of Excess Air
809 Ratio and Temperature on NO_x Emission From Grate Combustion of Biomass in the
810 Staged Air Combustion Scenario. *Energy Fuels* **2011**, 25 (10), 4643–4654.
- 811 (35) Kirch, T.; Birzer, C. H.; Medwell, P. R.; Holden, L. The Role of Primary and Secondary
812 Air on Wood Combustion in Cookstoves. *International Journal of Sustainable Energy*
813 **2018**, 37 (3), 268–277.
- 814 (36) Elmquist, M.; Cornelissen, G.; Kukulska, Z.; Gustafsson, Ö. Distinct Oxidative
815 Stabilities of Char Versus Soot Black Carbon: Implications for Quantification and
816 Environmental Recalcitrance. *Global Biogeochem. Cycles* **2006**, 20 (2), 1–11.
- 817 (37) Jiang, M.; Wu, Y.; Lin, G.; Xu, L.; Chen, Z.; Fu, F. Pyrolysis and Thermal-Oxidation
818 Characterization of Organic Carbon and Black Carbon Aerosols. *Science of the Total*
819 *Environment* **2011**, 409 (20), 4449–4455.
- 820 (38) Bond, T. C.; Doherty, S. J.; Fahey, D. W. Bounding the Role of Black Carbon in the
821 Climate System: a Scientific Assessment. *J. Geophys. Res. Atmos.* **2013**, 118 (11), 5380–
822 5552.
- 823 (39) Obaidullah, M.; Bram, S.; Verma, V. K.; De Ruyck, J. A Review on Particle Emissions
824 From Small Scale Biomass Combustion. *International Journal of Renewable Energy*
825 *Research* **2012**, 2 (1), 147–159.
- 826 (40) Garland, C.; Delapena, S.; Prasad, R.; L'Orange, C.; Alexander, D.; Johnson, M. Black
827 Carbon Cookstove Emissions: a Field Assessment of 19 Stove/Fuel Combinations.

- 828 *Atmospheric Environment* **2017**, *169*, 140–149.
- 829 (41) Tissari, J.; Lyyränen, J.; Hytönen, K.; Sippula, O.; Tapper, U.; Frey, A.; Saarnio, K.;
830 Pennanen, A. S.; Hillamo, R.; Salonen, R. O.; Hirvonen, M. R.; Jokiniemi, J. Fine
831 Particle and Gaseous Emissions From Normal and Smouldering Wood Combustion in a
832 Conventional Masonry Heater. *Atmospheric Environment* **2008**, *42* (34), 7862–7873.
- 833 (42) Torvela, T.; Tissari, J.; Sippula, O.; Kaivosoja, T.; Leskinen, J.; Virén, A.; Lähde, A.;
834 Jokiniemi, J. Effect of Wood Combustion Conditions on the Morphology of Freshly
835 Emitted Fine Particles. *Atmospheric Environment* **2014**, *87*, 65–76.
- 836 (43) Obernberger, I.; Brunner, T.; Barnthaler, G. *Fine Particulate Emissions From Modern*
837 *Austrian Small-Scale Biomass Combustion Plants*, 15th European Biomass Conference
838 & Exhibition, Berlin, Germany, May 7-11 2007.
- 839 (44) Nielsen, I. E.; Eriksson, A. C.; Lindgren, R.; Martinsson, J.; Nyström, R.; Nordin, E. Z.;
840 Sadiktsis, I.; Boman, C.; Nøjgaard, J. K.; Pagels, J. Time-Resolved Analysis of Particle
841 Emissions From Residential Biomass Combustion - Emissions of Refractory Black
842 Carbon, PAHs and Organic Tracers. *Atmospheric Environment* **2017**, *165*, 179–190.
- 843 (45) Champier, D.; Bédécarrats, J. P.; Kousksou, T.; Rivaletto, M.; Strub, F.; Pignolet, P.
844 Study of a TE (Thermoelectric) Generator Incorporated in a Multifunction Wood Stove.
845 *Energy* **2011**, *36* (3), 1518–1526.
- 846 (46) Champier, D.; Bedecarrats, J. P.; Rivaletto, M.; Strub, F. Thermoelectric Power
847 Generation From Biomass Cook Stoves. *Energy* **2010**, *35* (2), 935–942.
- 848 (47) Gao, H. B.; Huang, G. H.; Li, H. J.; Qu, Z. G.; Zhang, Y. J. Development of Stove-
849 Powered Thermoelectric Generators: a Review. *Applied Thermal Engineering* **2016**, *96*,

- 850 297–310.
- 851 (48) Nuwayhid, R. Y.; Shihadeh, A.; Ghaddar, N. Development and Testing of a Domestic
852 Woodstove Thermoelectric Generator with Natural Convection Cooling. *Energy
853 Conversion and Management* **2005**, *46* (9-10), 1631–1643.
- 854 (49) Mal, R.; Prasad, R.; Vijay, V. K.; Verma, A. R. The Design, Development and
855 Performance Evaluation of Thermoelectric Generator(TEG) Integrated Forced Draft
856 Biomass Cookstove. *Procedia - Procedia Computer Science* **2015**, *52*, 723–729.
- 857 (50) Digi-Key Electronics. Fans and Thermal Management: DC Brushless Fans (BLDC).
858 [http://www.digikey.com/products/en/fans-thermal-management/dc-brushless-fans-blcdc/
859 217?](http://www.digikey.com/products/en/fans-thermal-management/dc-brushless-fans-blcdc/217?) (accessed September 12, 2018).
- 860 (51) Valavanidis, A.; Fiotakis, K.; Vlachogianni, T. Airborne Particulate Matter and Human
861 Health: Toxicological Assessment and Importance of Size and Composition of Particles
862 for Oxidative Damage and Carcinogenic Mechanisms. *Journal of Environmental Science
863 and Health, Part C* **2008**, *26* (4), 339–362.
- 864 (52) Martins, L. D.; Martins, J. A.; Freitas, E. D.; Mazzoli, C. R.; Gonçalves, F. L. T.; Ynoue,
865 R. Y.; Hallak, R.; Albuquerque, T. T. A.; Andrade, M. de F. Potential Health Impact of
866 Ultrafine Particles Under Clean and Polluted Urban Atmospheric Conditions: a Model-
867 Based Study. *Air Qual Atmos Health* **2010**, *3* (1), 29–39.
- 868 (53) Chen, R.; Bin Hu; Liu, Y.; Xu, J.; Yang, G.; Xu, D.; Chen, C. Beyond PM2.5: the Role
869 of Ultrafine Particles on Adverse Health Effects of Air Pollution. *BBA - General
870 Subjects* **2016**, *1860* (12), 2844–2855.
- 871 (54) Clifford, S.; Mazaheri, M.; Salimi, F.; Ezz, W. N.; Yeganeh, B.; Low-Choy, S.; Walker,

- 872 K.; Mengersen, K.; Marks, G. B.; Morawska, L. Effects of Exposure to Ambient
873 Ultrafine Particles on Respiratory Health and Systemic Inflammation in Children.
874 *Environment International* **2018**, *114*, 167–180.
- 875 (55) Just, B.; Rogak, S.; Kandlikar, M. Characterization of Ultrafine Particulate Matter From
876 Traditional and Improved Biomass Cookstoves. *Environ. Sci. Technol.* **2013**, *47* (7),
877 3506–3512.
- 878 (56) Shen, G.; Gaddam, C. K.; Ebersviller, S. M.; Vander Wal, R. L.; Williams, C.; Faircloth,
879 J. W.; Jetter, J. J.; Hays, M. D. A Laboratory Comparison of Emission Factors, Number
880 Size Distributions, and Morphology of Ultrafine Particles From 11 Different Household
881 Cookstove-Fuel Systems. *Environ. Sci. Technol.* **2017**, *51* (11), 6522–6532.
- 882 (57) Kelz, J.; Brunner, T.; Obernberger, I.; Jalava, P.; Hirvonen, M. R. *PM Emissions From*
883 *Old and Modern Biomass Combustion Systems and Their Health Effects*, Proceedings of
884 the 18th European Biomass Conference, Lyon, France, May 2010; ETA - Florence
885 Renewable Energies: Florence, Italy, 2010.
- 886 (58) Johansson, L. S.; Leckner, B.; Gustavsson, L.; Cooper, D.; Tullin, C.; Potter, A.
887 Emission Characteristics of Modern and Old-Type Residential Boilers Fired with Wood
888 Logs and Wood Pellets. *Atmospheric Environment* **2004**, *38* (25), 4183–4195.
- 889 (59) Wiinikka, H.; Gebart, R. The Influence of Air Distribution Rate on Particle Emissions in
890 Fixed Bed Combustion of Biomass. *Combustion Science and Technology* **2005**, *177* (9),
891 1747–1766.
- 892 (60) Hosseini, S.; Li, Q.; Cocker, D.; Weise, D.; Miller, A.; Shrivastava, M.; Miller, J. W.;
893 Mahalingam, S.; Princevac, M.; Jung, H. Particle Size Distributions From Laboratory-

- 894 Scale Biomass Fires Using Fast Response Instruments. *Atmos. Chem. Phys.* **2010**, *10*
895 (16), 8065–8076.
- 896 (61) Fox, R. W.; McDonald; Pritchard, P. J. *Introduction to Fluid Mechanics*, 7 ed.; John
897 Wiley & Sons: Hoboken, 2017.
- 898 (62) Hay, N.; Spencer, A. Discharge Coefficients of Cooling Holes with Radiused and
899 Chamfered Inlets. *Journal of Turbomachinery* **1992**, *114* (701), 1–6.
- 900 (63) Taslim, M.; Ugarte, S. Discharge Coefficient Measurements for Flow Through
901 Compound-Angle Conical Holes with Cross-Flow. *The International Journal of*
902 *Rotating Machinery* **2004**, *10* (2), 145–153.
- 903 (64) Incropera, F.; Dewitt, D.; Bergman, T.; Levine, A. *Fundamentals of Heat and Mass*
904 *Transfer*, 6 ed.; John Wiley & Sons : Hoboken, 2007; pp 1–10.
- 905 (65) Frigge, M.; Hoaglin, D. C.; Iglewicz, B. Some Implementations of the Boxplot. *The*
906 *American Statistician* **1989**, *43* (1), 50–54.
- 907 (66) Hand, J. L.; Kreidenweis, S. M. A New Method for Retrieving Particle Refractive Index
908 and Effective Density From Aerosol Size Distribution Data. *Aerosol Science and*
909 *Technology* **2002**, *36* (10), 1012–1026.
- 910 (67) Pitz, M.; Schmid, O.; Heinrich, J.; Birmili, W.; Maguhn, J.; Zimmermann, R.;
911 Wichmann, H.-E.; Peters, A.; Cyrys, J. Seasonal and Diurnal Variation of PM_{2.5}
912 Apparent Particle Density in Urban Air in Augsburg, Germany. *Environ. Sci. Technol.*
913 **2008**, *42* (14), 5087–5093.
- 914 (68) Khlystov, A.; Stanier, C.; Pandis, S. N. An Algorithm for Combining Electrical Mobility
915 and Aerodynamic Size Distributions Data When Measuring Ambient Aerosol. *Aerosol*

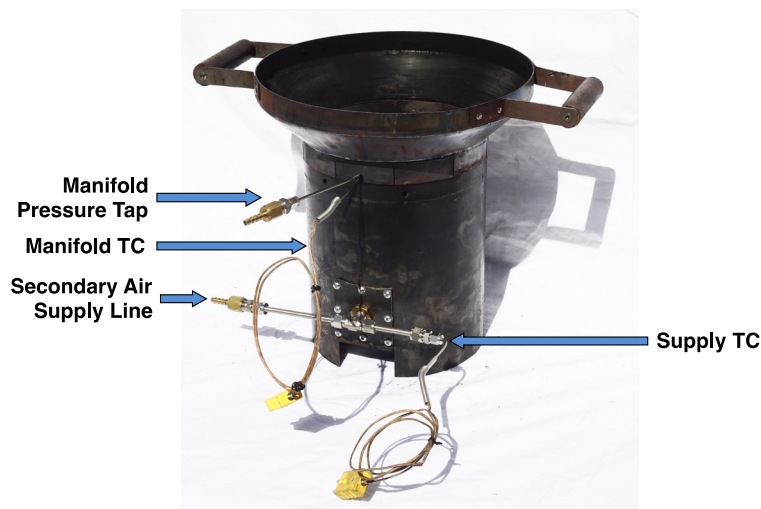
916 *Science and Technology* **2004**, 38 (S1), 229–238.

917

918 **Appendix A. Materials and Methods**

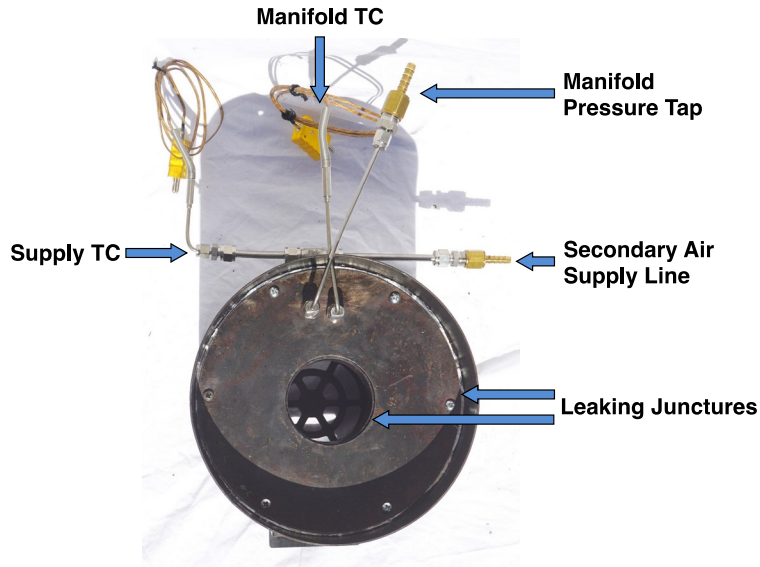
919 **A.1 Modular Air Injection Cookstove Design: Version 2 (MOD2)**

920 The MOD2 stove is a wood-burning cookstove that enables the experimental
921 optimization of secondary air injection design parameters. Figure A1 and Figure A2 below
922 provide a rear and top view of the MOD2 stove, respectively, showing the location of the
923 secondary air supply line, thermocouples, and manifold pressure port. Figure A2 also shows the
924 junctures at the top of the manifold that leaked during testing. The outer juncture was sealed with
925 a high-temperature graphite gasket (Figure A3(b)), but the thin top plate warped over extended
926 use and thermal cycling (Figure A3(a)), resulting in leakage. Figure A1 shows that secondary air
927 is injected into the manifold through a removable access port, which can be easily modified to
928 accommodate a small electric fan or blower in future studies.



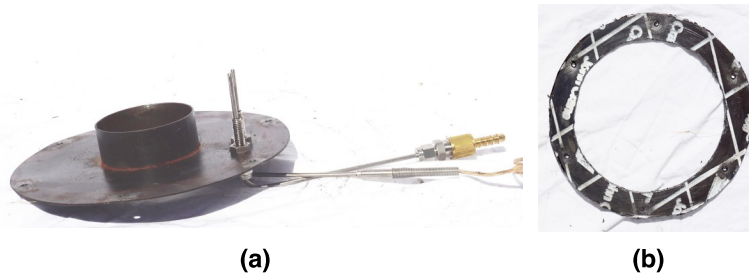
929

930 **Figure A1.** Rear view of the MOD2 stove, showing the secondary air inlet, thermocouples (TC),
931 and manifold pressure port.



932

933 **Figure A2.** Top view of the MOD2 stove, showing the secondary air inlet, thermocouples (TC),
 934 manifold pressure port, and the leaky manifold junctures. The pot skirt and pot supports were
 935 removed so as to expose the top of the manifold assembly.



936

937 **Figure A3.** (a) Top of the manifold assembly, showing the thermocouple and pressure port that
 938 extend into the manifold. (b) High temperature graphite gasket, used to seal the outer juncture
 939 between the top of the manifold assembly and the stove body.

940 **A.2 Preliminary Testing Procedure**

941 Over the course of 52 preliminary tests, a total of 7 injection patterns were evaluated at
 942 secondary flow rates ranging from 14 to 43 SLPM (the total flow into the stove manifold). For all

943 patterns, the air injection orifices had a diameter of 1.59 mm (0.0625 in). Primary air flow was
944 controlled using adjustable intakes located under the grate. During the first 8 tests, a constant
945 firepower setting of 4 to 5 kW was difficult to maintain and the combustion efficiency was low,
946 thereby indicating that the stove lacked primary air. Consequently, the adjustable air intakes
947 below the grate were fully opened, and when this did not prove sufficient, the stove was also
948 elevated on three bricks, such that primary air could flow more freely through the grate and into
949 the bottom of the firebox. The stove was operated in this configuration for the remaining 44 trials
950 of the preliminary testing phase.

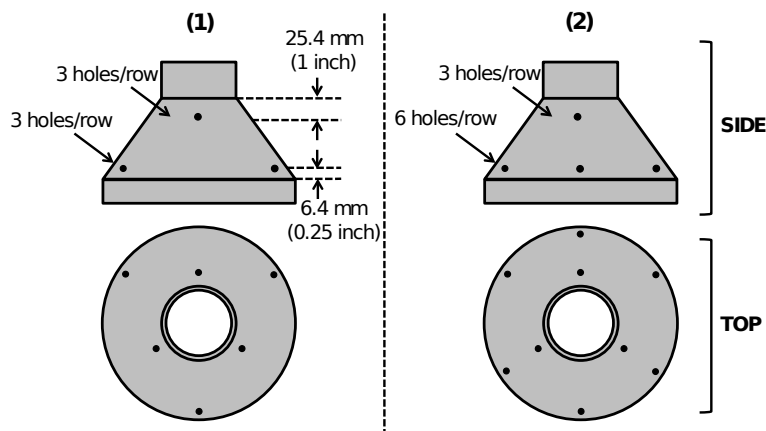
951 In order to modulate the height of the pot above the chimney throat, 2.5-mm (0.10-inch)
952 thick washers were added under the three bolts that serve as pot supports. For 17 of the first 18
953 tests, the stove was operated with two washers stacked under the pot support. However, as the air
954 injection flow rate and pattern were modulated to reduce emissions, thermal efficiency tended to
955 suffer. As a result, the supports were reduced to a single washer for all remaining trials, in an
956 effort to maximize heat transfer to the pot. The stove was not fitted with a pot skirt or
957 thermocouples during preliminary testing, and so no secondary air temperature data were
958 collected.

959 **A.3 Parametric Testing Procedure**

960 Using the data collected during the preliminary testing phase, two promising air injection
961 patterns were identified for further parametric testing (as outlined in Appendix B.1). Pattern 1
962 consisted of two concentric rows, each with three orifices evenly spaced around the
963 circumference of the conical chimney. The bottom row of orifices were located ~6.4 mm (0.25
964 inch) above the juncture of the conical chimney and firebox, while the top row was located ~25

965 mm (1.0 inch) below the throat. The orifices in each row were offset, such that orifices in the top
966 row were exactly above the midpoint between two orifices in the bottom row. Pattern 2 was
967 identical to Pattern 1, except that the bottom row had six evenly spaced orifices, rather than
968 three. The two rows in Pattern 2 were vertically aligned, such that orifices in the top row were
969 directly above every other orifice in the bottom row. Both patterns are shown in Figure A4.

970 During the first 13 parametric tests, the height of the pot above the chimney throat was
971 incrementally increased from ~1.59 to 2.5 cm (~ 0.625 to 1.0 inch) to reduce the impingement of
972 flames on the bottom of the pot, but was not increased past this set point so as to enhance thermal
973 performance (larger gaps between the pot and skirt diminish convective heat transfer from the
974 exhaust gases). For the remaining 47 trials, the pot height was held constant at 2.5 cm (1.0 inch)
975 using three washers stacked under each of the bolt supports. Throughout the parametric testing
976 phase, the primary air intake was set to the fully open position. Due to fears that the stove may
977 have tipped over when elevated on three refractory bricks, 11 of the 59 parametric tests were
978 conducted with the stove placed on a piece of sheet metal. However, the stove did not seem more
979 stable in this configuration, and so all other tests were conducted using the three bricks for the
980 sake of consistency.

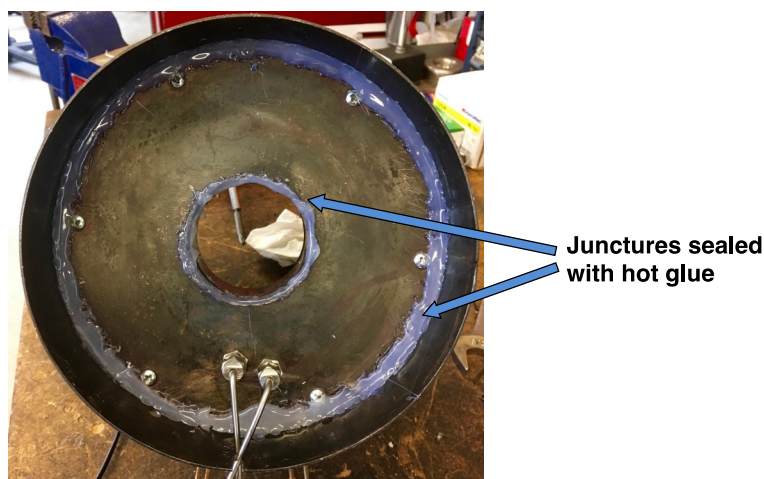


981

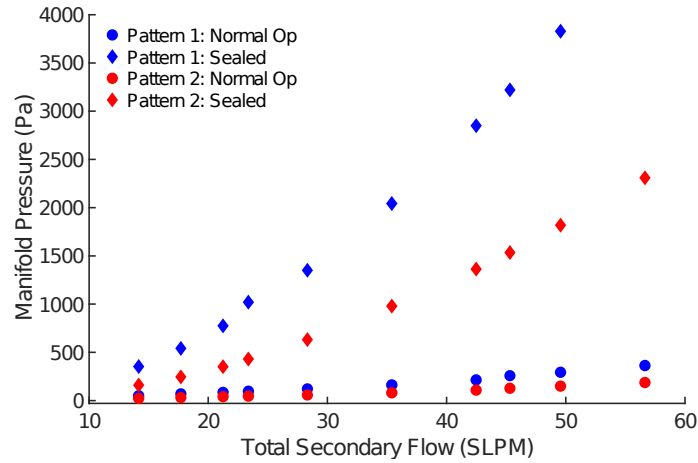
982 **Figure A4.** Schematic representation of the two injection patterns (Pattern 1 and Pattern 2)
983 identified during preliminary testing, and evaluated through parametric testing. All air injection
984 orifices have a diameter of 1.59 mm (0.0625 inch). Schematic is not drawn to scale.

985 **A.4 Manifold Leakage Correction**

986 The MOD2 stove's integrated manifold had some faulty juncture seals (Figure A2), and
987 so a portion of the secondary air systematically leaked to the environment, rather than flowing
988 through the orifices in the injection pattern and into the combustion chamber (firebox). While the
989 stove was cold, the manifold was completely sealed using hot glue (Figure A5) to calculate the
990 portion of the secondary flow injected through the orifices. For the two air injection patterns
991 identified during preliminary testing, Figure A6 shows the manifold pressure at secondary flow
992 rates ranging from 14 to 57 SLPM, with the manifold both in the normal operating configuration
993 (leaking) and fully sealed using hot glue. Manifold pressure measurements were collected with
994 the stove at ambient conditions throughout. Figure A6 shows that for both air injection patterns,
995 the manifold pressure was much greater once the junctures were sealed with hot glue.



996
997 **Figure A5.** Top of the manifold assembly, sealed with hot glue.



998

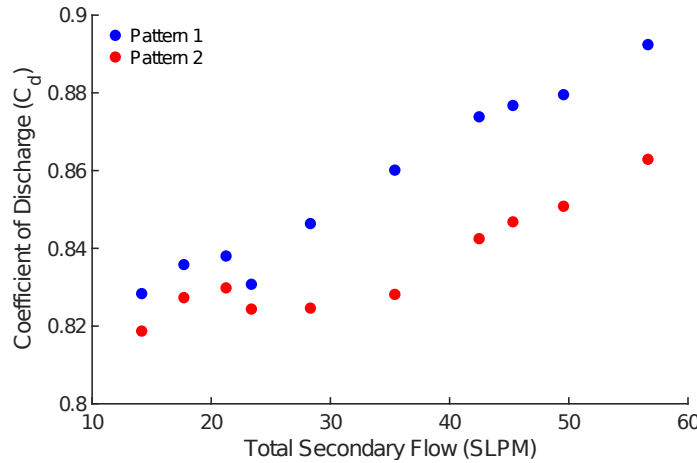
999 **Figure A6.** Manifold pressure as a function of secondary air flow rate for two injection patterns,
 1000 with the manifold in both the normal operating configuration (leaking) and fully sealed using hot
 1001 glue.

1002 With the stove manifold completely sealed and all the secondary air passing through the
 1003 injection pattern, it was possible to use the corresponding pressure and flow rate measurements
 1004 to calculate the coefficient of discharge (C_d) through the orifices using Equation A1,

1005
$$C_d = \left(\frac{4Q}{N\pi D^2} \right) \sqrt{\frac{\rho_{STP}}{2\Delta P}} \quad (A1)$$

1006 where Q is the standard volumetric flow rate of secondary air (SLPM), ρ_{STP} is the density of air at
 1007 standard conditions (1.225 kg/m^3), ΔP is the gauge pressure in the manifold (Pa), N is the
 1008 number of orifices in the injection pattern, and D is the orifice diameter (1.59 mm).⁶¹ The
 1009 standard volumetric flow rate of secondary air into the manifold was measured with a rotameter
 1010 (SLPM), and so must correspondingly be converted to mass flow rate using the density of air at
 1011 standard conditions. Figure A7 below shows the coefficient of discharge calculated at each
 1012 parametric setting (with the manifold fully sealed). The coefficient of discharge remains
 1013 relatively constant throughout, ranging from 0.82 to 0.88, and has an average value of $0.846 \pm$

1014 0.008 (mean of C_d at all parametric configurations \pm 90% confidence interval). This value of
 1015 discharge coefficient agrees closely with that derived in other experimental studies of turbulent
 1016 air discharge through small orifices.^{62,63}



1017
 1018 **Figure A7.** Coefficient of discharge (C_d) calculated at each parametric configuration, using
 1019 pressure and flow rate measurements collected with the MOD2 stove manifold fully sealed, such
 1020 that all the secondary air passes through orifices in each of the two injection patterns presented.

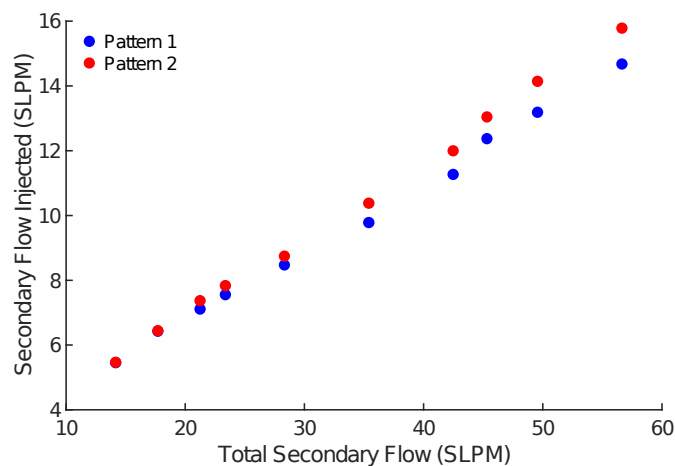
1021 Using the average coefficient of discharge calculated above (0.846 ± 0.008) and the
 1022 manifold pressure measurements collected in the normal operating configuration (with the
 1023 leakage), it was possible to determine the standard volumetric flow rate of secondary air passing
 1024 through each injection pattern as follows,

1025
$$Q = \left(\frac{C_d N \pi D^2}{4} \right) \sqrt{\frac{2 \Delta P}{\rho_{air}}}. \quad (A 2)$$

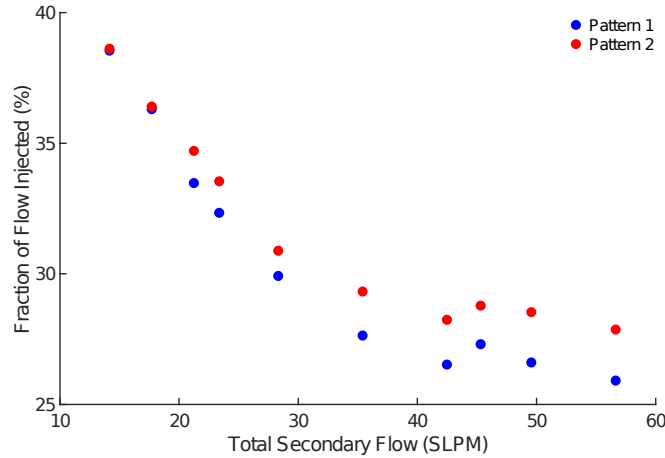
1026 For each combination of secondary flow rate (the total flow into the manifold) and injection
 1027 pattern, Figure A8 and Figure A9 show the standard volumetric flow rate (SLPM) and fraction
 1028 (%) of secondary air injected into the firebox, respectively. The flow rate of injected air increased
 1029 linearly with total secondary flow, and was generally consistent between the two patterns at each

1030 setting. As total secondary flow increased, the fraction of injected air initially decreased from
1031 39% to 27%, presumably because higher manifold pressures pushed against the top of the
1032 manifold assembly and expanded the cracks through which air is leaking. However, the leakage
1033 stabilized for flow rates > 40 SLPM, as the cracks could expand no further.

1034 Using these calculations, it was possible to present the stove performance results in terms
1035 of the standard volumetric flow injected through the patterns, rather than the total secondary flow
1036 into the manifold. Since secondary air leaked mostly through the outer juncture at the top of the
1037 manifold assembly, away from the firebox, it was unlikely that the leakage significantly impacted
1038 the stove's combustion performance. However, it should be acknowledged that the leakage of
1039 cold secondary air near the pot of water (the thermal load) may have hampered heat transfer from
1040 the hot exhaust flow, and potentially restricted the stove's thermal performance. Future iterations
1041 of the MOD stove should rectify the leakages, and manifold pressure measurements should be
1042 collected in real time throughout testing (as was done for temperature).



1043
1044 **Figure A8.** Standard volumetric flow rate of air injected through the orifices in each injection
1045 pattern, calculated using Equation A2, as a function of total secondary flow rate into the
1046 manifold.



1047

1048 **Figure A9.** Fraction of the total secondary flow rate injected through the orifices in each air
 1049 injection pattern.

1050 **A.5 Data Analysis and Performance Metrics**

1051 Performance metrics, such as firepower, equivalent dry mass of fuel consumed, and
 1052 thermal efficiency are calculated for each test using the methods provided in the WBT Protocol
 1053 4.2.3.²⁹

1054 Emission factors are calculated according to the methods outlined by Caubel et al.,²⁰ and
 1055 some additional methods are presented below. The total mass of gaseous emissions emitted (CO,
 1056 CO₂) or consumed (O₂) is calculated using Equation A3 below,

1057
$$m_{gas} = \sum_{t=0}^{t=t_f} \frac{10^6 \times MW (C_{gas}(t) - C_{gas,bkg}) Q_{duct}(t) P_{amb} \Delta t}{R(T_{duct}(t) + 273)} \quad (A3)$$

1058 where m_{gas} (g) is the total mass of gaseous emissions, t is the time step, t_f is the duration of the
 1059 cold start test (sec), C_{gas} is the volumetric gas concentration (ppmv), $C_{gas,bkg}$ is the background
 1060 gas concentration (ppmv), MW is the molecular weight of the gas species (g/mol), Q_{duct} is the
 1061 duct flow rate (m³/sec), P_{amb} is the ambient pressure (97150 Pa at the laboratory's altitude of
 1062 ~300 m MSL), Δt is the sampling period (1 sec), R is the ideal gas constant (8.314 J/ (mol K)),

1063 and T_{duct} is the temperature in the duct ($^{\circ}\text{C}$). The background levels of each gas species are
 1064 calculated by taking the average of concentration measurements collected for 1 min prior to the
 1065 start of the test phase (ignition of the kindling), while the system is sampling ambient air.
 1066 Background concentrations of $\text{PM}_{2.5}$ and BC are always assumed to be exactly $0 \mu\text{g}/\text{m}^3$.

1067 The average standard volumetric flow rate of air stoichiometrically consumed by the
 1068 combustion (Q_{stoich} , SLPM) is calculated using Equation A4 below,

$$1069 \quad Q_{stoich} = \frac{4.76 m_{O_2} (MW_{air} / MW_{O_2})}{\rho_{STP} t t b} \quad (A4)$$

1070 where m_{O_2} is the total mass of O_2 consumed over the cold start (g, calculated using Equation A3),
 1071 MW_{air} is the molecular of air (28.97 g/mol), MW_{O_2} is the molecular mass of O_2 (32.0 g/mol), and
 1072 $t t b$ is the time to boil (min). Throughout the cold start test, the air injection velocity (v , m/s) is
 1073 calculated at every time step (t) using Equation A5,

$$1074 \quad v(t) = \frac{4 \rho_{STP} Q}{\rho(t) \pi N D^2} = \frac{4 \rho_{STP} Q (T_{man}(t) + 273) R_{air}}{P_{man} \pi N D^2} \quad (A5)$$

1075 where ρ is the density of air in the manifold (kg/m^3), T_{man} is the air temperature in the manifold
 1076 ($^{\circ}\text{C}$), R_{air} is the ideal gas constant for air (287 J/Kg K), and P_{man} is the absolute pressure in the
 1077 manifold (roughly equal to the local ambient pressure, 97150 Pa). Similarly, the manifold gauge
 1078 pressure (ΔP , Pa) is calculated using Equation 1. The average secondary air velocity and
 1079 manifold pressure are evaluated using one-second values calculated over the length of the cold
 1080 start air. The average rate of heat transferred to the secondary air in the manifold (H_{man} , kW) is
 1081 calculated using,

$$1082 \quad H_{man} = \rho_{STP} Q \left(C_p (T_{man,avg} - T_{i,avg}) + \frac{1}{2} (4 \rho_{STP} Q R_{air})^2 \left(\left(\frac{(T_{man,avg} + 273)}{P_{amb} (N \pi D^2)} \right)^2 - \left(\frac{(T_{i,avg} + 273)}{P_{man} (\pi D_i^2)} \right)^2 \right) \right) \quad (A6)$$

1083

1084 where C_p is the specific heat of air (1.055 KJ/Kg K), D_{in} is the secondary air inlet diameter (4.6
1085 mm), and $T_{man,avg}$ and $T_{in,avg}$ are the average secondary air temperatures in the manifold and inlet
1086 (°C), respectively, over the length of the test.⁶⁴

1087 Multiple tests were conducted for each parametric stove design configuration (unique
1088 combination of secondary air injection pattern and flow rate), and the first and third quartiles ($Q1$
1089 and $Q3$) were calculated for each replicate set of results. Outliers in each replicate set are defined
1090 as,

$$1091 \quad Q1 - 1.5 IQR > outlier > Q3 + 1.5 IQR \quad (A7)$$

1092 where IQR is the interquartile range ($= Q3 - Q1$).⁶⁵ Outliers are removed from the replicate set
1093 according to this criterion, and for each stove design configuration, the mean and 90%
1094 confidence interval of the remaining measurements (or calculated metrics) is evaluated.

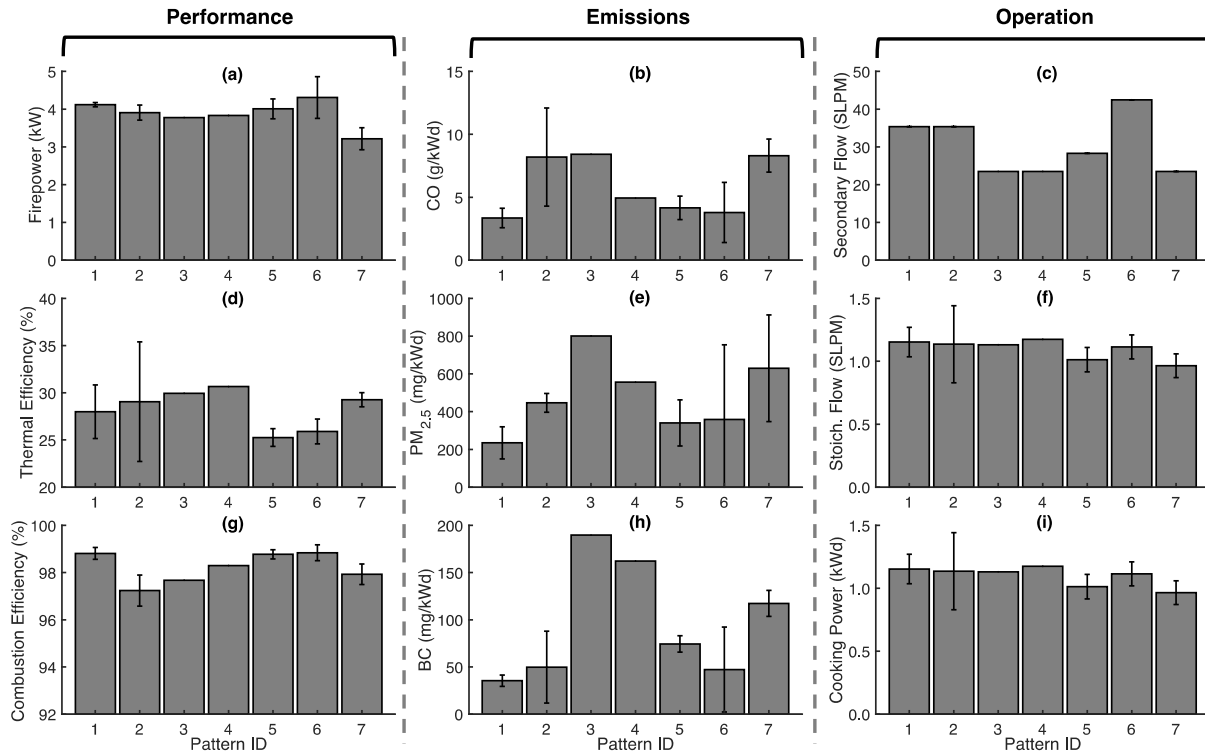
1095 Using size-resolved particle emission measurements from the TSI 3321 APS and TSI
1096 3091 FMPS, particle density was iteratively calculated to be $1.90 \pm 0.05 \text{ g/cm}^3$ (mean of particle
1097 density calculated for all 59 parametric stove tests $\pm 90\%$ confidence interval) according to the
1098 methods presented by Caubel et al.²⁰ This density value agrees closely with that calculated by
1099 other researchers.^{66,67} APS measurements are converted from aerodynamic to electrical mobility
1100 diameter using the calculated particle density,⁶⁸ and combined with FMPS measurements. FMPS
1101 measurements span from 6 to 340 nm, while APS measurements span from 393 to 2500 nm. The
1102 last three bins of the FMPS measurement span (from 393 to 524 nm) were discarded.

1103 **Appendix B: Supplemental Results and Discussion**

1104 **B.1 Preliminary Testing Results**

1105 Testing results from all preliminary trials are provided on the first sheet of the data file
1106 entitled 'MOD2_test_results.xlsx'. The data file provides the performance and emissions metrics
1107 calculated for each individual test, and catalogs all parametric stove design configurations
1108 evaluated. In the data file, metrics highlighted in red represent outlier values not used in the
1109 calculation of configuration-average metrics (at most, only one outlier was ever removed from
1110 each set of replicate metric values). For this test phase, a total of 4 individual data points were
1111 removed from the replicate sets of measurements or output metrics. Manifold pressure
1112 measurements were only collected with air injection patterns 1 and 2, and so some operational
1113 metrics are unavailable for the remaining patterns (e.g. the calculated portion of secondary flow
1114 rate of air injected through the orifices into the firebox).

1115 Figure B1 summarizes the thermal and emissions performance of each air injection
1116 pattern evaluated during the preliminary testing phase. For each air injection pattern, average
1117 metrics are provided for the secondary flow rate setting with the most replicate trials, shown in
1118 Figure B1(c) (please note that this represents the total secondary flow into the manifold, not the
1119 calculated portion of the flow actually injected through the orifices). Injection patterns were not
1120 systematically evaluated for a static set of secondary flow rates to reduce the total number of
1121 preliminary trials. For example, patterns were initially evaluated at secondary flow rates ranging
1122 from 18.9 to 23.5 SLPM, but it became evident that more secondary flow was required to
1123 achieve meaningful emissions reductions, and so later trials range from 28.3 to 42.5 SLPM.
1124 Although this approach reduces the comparability of the results, it allows the parametric space to
1125 be constrained rapidly prior to more methodical testing.



1126

1127 **Figure B1.** MOD2 stove performance, emissions, and operational metrics during high-power
 1128 cold start testing (preliminary tests), presented for each air injection pattern at single secondary
 1129 flow rate setting: (a) Firepower (kW); (b) CO emissions (g/KWd); (c) Total secondary flow rate
 1130 into the manifold (SLPM); (d) Thermal Efficiency (%); (e) PM_{2.5} emissions (mg/KWd); (f)
 1131 Stoichiometric flow rate of air into the combustion (SLPM); (g) Combustion Efficiency (%); (h)
 1132 BC emissions (mg/KWd); (i) Cooking Power (KWd). Bars represent the mean of replicate test
 1133 data collected for each stove configuration, while error bars represent the corresponding 90%
 1134 confidence interval. Only 1 test was conducted for some configurations (Patterns 3 and 4), and so
 1135 confidence intervals are not shown.

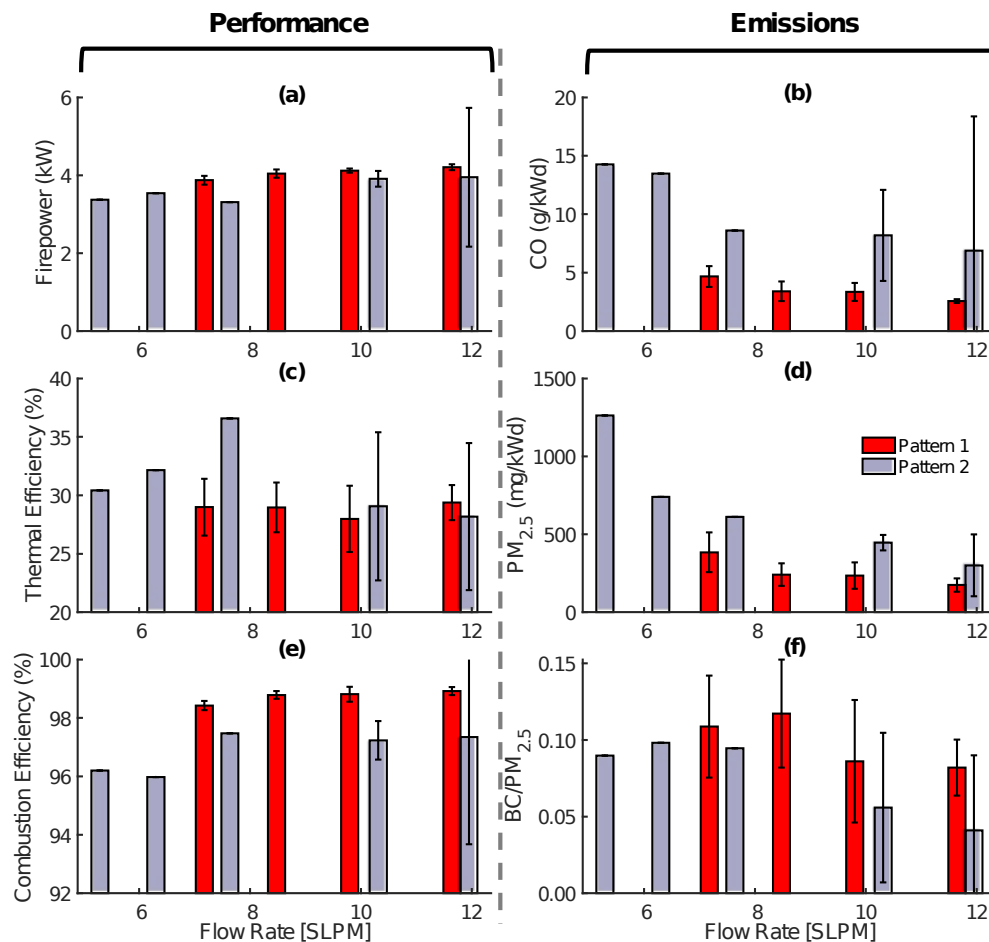
1136 Patterns 3 and 4 only had injection orifices in the bottom row (closest to the fuel bed).
 1137 Visible mixing of the flame was minimal and the air jets seemed to impinge directly onto the fuel

1138 bed. As a result, these patterns had very high BC emissions (Figure B1(h)) and were abandoned
1139 after a single experimental trial. Similarly, Pattern 7 was not considered for further testing
1140 because of elevated emissions. Pattern 7 has twelve air injection orifices, and so further testing at
1141 higher flow rates was not pursued as we sought to achieve higher air injection velocities and
1142 promote more turbulent mixing (with this aim in mind, all other injection patterns have ≤ 9 air
1143 injection orifices). Patterns 5 and 6 approach order-of-magnitude emissions reductions relative to
1144 the TSF, but thermal efficiency is low ($\sim 25\%$). Further emissions reductions would require
1145 higher secondary flow rates, which in turn would likely reduce the thermal efficiency to
1146 unacceptable levels (the thermal efficiency of the TSF is $\sim 23\%$). As a result, Patterns 5 and 6
1147 were not considered for further evaluation.

1148 Pattern 1 was chosen for the parametric testing phase, as it had the lowest CO, PM_{2.5}, and
1149 BC mass emissions and maintained high thermal efficiency ($\sim 28\%$). Pattern 2 is nearly identical
1150 to Pattern 1, with only three additional orifices in the bottom row of the injection pattern.
1151 Although Pattern 2 has higher emissions than Pattern 1, it also achieves higher thermal
1152 efficiencies ($\sim 29\%$). Pattern 2 was chosen for the parametric testing phase so that the results
1153 could be compared to those from Pattern 1, and to illuminate whether the placement of air
1154 injection holes leads to a trade-off between maximizing thermal efficiency and minimizing
1155 harmful pollutant emissions. The configuration-average data presented in Figure B1 is
1156 enumerated on the first sheet of the data file entitled 'MOD2_test_summary.xlsx', and the
1157 number of replicate tests conducted for each configuration is provided.

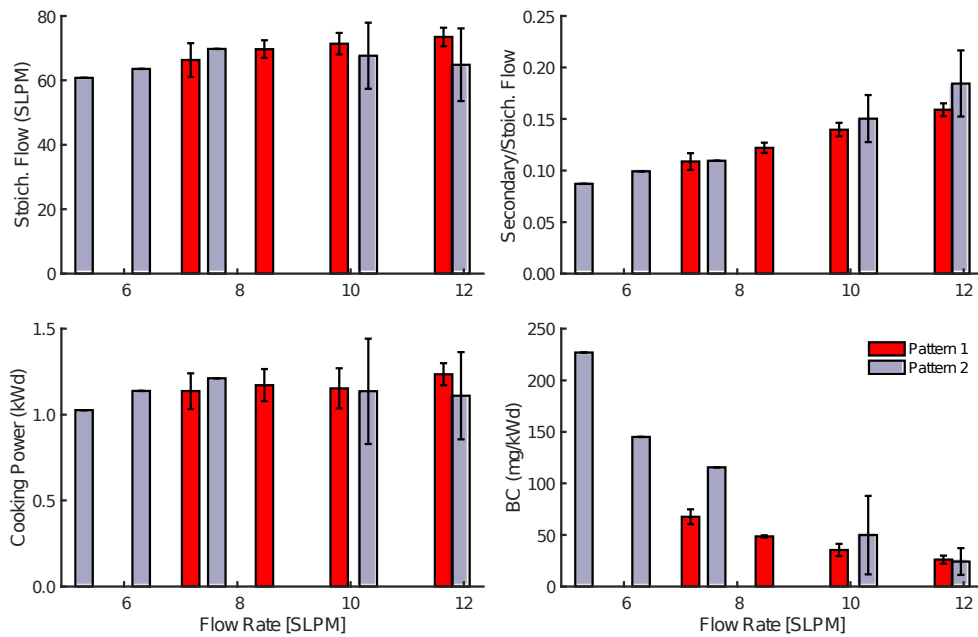
1158 Figure B2 and Figure B3 below summarize all the preliminary testing results collected
1159 with air injection patterns 1 and 2. For Pattern 1, 5 to 8 replicate tests were conducted at four
1160 flow rate settings, ranging from 7.2 to 12 SLPM. Only 1 or 2 tests were conducted at each of five

1161 flow rate settings using Pattern 2, and so the corresponding confidence intervals are large or non-
 1162 existent. When comparing results from the preliminary and parametric testing phases, only
 1163 results collected with Pattern 1 should be considered, as insufficient trials were conducted with
 1164 Pattern 2. Since thermocouples were not installed during preliminary testing, some temperature
 1165 dependent parameters are omitted, such as average air injection velocity. The configuration-
 1166 average data presented in Figure B2 and Figure B3 is enumerated on the first sheet of the data
 1167 file entitled 'MOD2_test_summary.xlsx', and the number of replicate tests conducted for each
 1168 configuration is provided.



1169
 1170 **Figure B2.** MOD2 stove performance, emissions, and operational metrics during high-power
 1171 cold start testing (preliminary tests), presented as function of secondary air injection flow rate

1172 and pattern: (a) Firepower (kW); (b) CO emissions (g/KWd); (c) Thermal Efficiency (%); (d)
 1173 PM_{2.5} emissions (mg/KWd); (e) Combustion Efficiency (%); (f) BC emissions (mg/KWd);. Bars
 1174 represent the mean of replicate test data collected for each stove configuration, while error bars
 1175 represent the corresponding 90% confidence interval. Only 1 test was conducted for some
 1176 configurations (Pattern 2), and so confidence intervals are not shown.

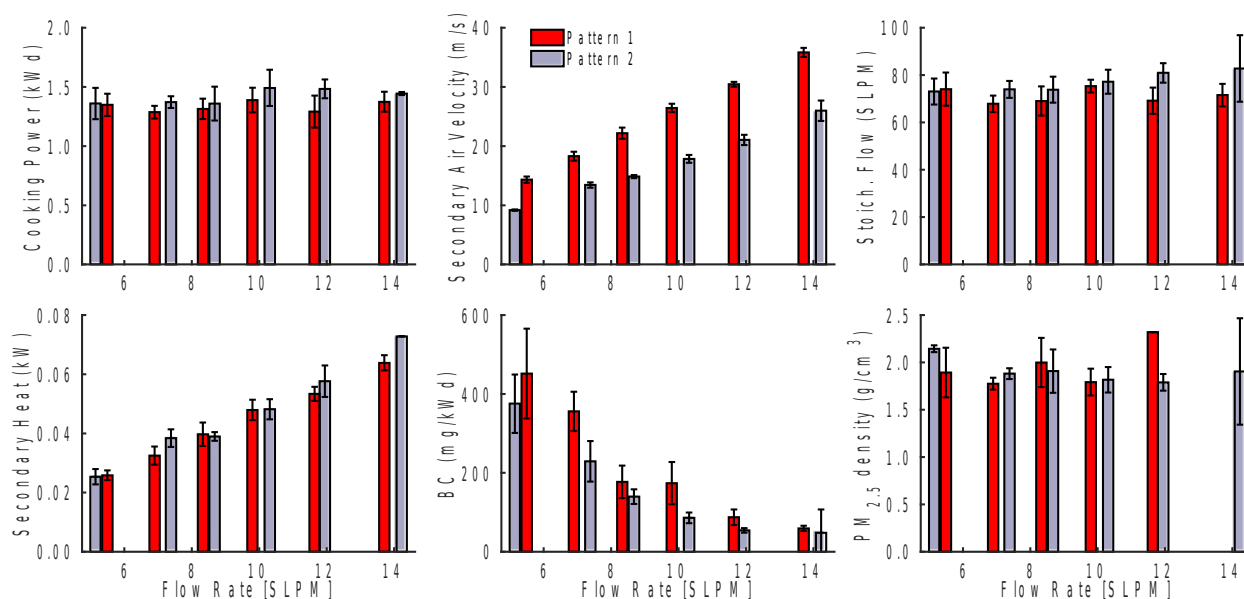


1177

1178 **Figure B3.** MOD2 stove operational metrics during high-power cold start testing (preliminary
 1179 tests), presented as function of secondary air injection flow rate and pattern: (a) Stoichiometric
 1180 flow rate of air into the combustion (SLPM); (b) Ratio of the secondary to stoichiometric flow
 1181 rate of air; (c) Cooking Power (KWd); (d) BC emissions (mg/KWd). Bars represent the mean of
 1182 replicate test data collected for each stove configuration, while error bars represent the
 1183 corresponding 90% confidence interval. Only 1 test was conducted for some configurations
 1184 (Pattern 2), and so confidence intervals are not shown.

1185 B.2 Parametric Testing Results

1186 During parametric testing, two air injection patterns were evaluated at six flow rate
1187 settings. Testing results from all parametric trials are provided on the second sheet of the data file
1188 entitled 'MOD2_test_results.xlsx'. In the data file, metrics highlighted in red represent outlier
1189 values not used in the calculation of configuration-average metrics (at most, only one outlier was
1190 ever removed from each set of replicate metric values). For this test phase, a total of 10
1191 individual data points were removed from the replicate sets of measurements or output metrics.
1192 In addition to Figure 2 in the manuscript, Figure B4 summarizes the stove's performance at all
1193 twelve parametric design configurations. The configuration-average data presented in Figure 2
1194 and Figure B4 are enumerated on the second sheet of the data file entitled
1195 'MOD2_test_summary.xlsx', and the number of replicate tests conducted for each configuration
1196 is provided.



1197
1198 **Figure B4.** MOD2 stove performance, emissions, and operational metrics during high-power
1199 cold start testing, presented as function of secondary air injection flow rate and pattern: (a)

1200 Cooking Power (kWd); (b) Average secondary air injection velocity (m/s); (c) Stoichiometric
 1201 flow rate of air into the combustion (SLPM); (d) Average rate of heat transfer to secondary air in
 1202 the manifold (kW); (e) Black carbon (BC) emissions (mg/kWd); (f) PM_{2.5} density (g/cm³). Bars
 1203 represent the mean of replicate test data collected for each stove configuration, while error bars
 1204 represent the corresponding 90% confidence interval. Error bars necessarily are omitted for
 1205 metrics calculated from a single data point.

1206

1207 **B.3 Optimal MOD2 Stove and TSF Comparison**

1208 Table B1 below summarizes the performance of the MOD2 using secondary air injection
 1209 Pattern 2 at a flow rate of 12 SLPM, and compares it to a traditional three stone fire (TSF).
 1210 Testing results for the TSF are provided by Rapp et al., and were collected using the same
 1211 experimental set up and methods as that used during MOD2 stove testing.²¹

	TSF	MOD2	Difference (%)
Number of Tests	10	4	N/A
Firepower (kW)	5.3 (0.4)	4.7 (0.2)	-11 (8)
Time to boil (min)	31 (3)	24 (2)	-20 (10)
Cooking Power (kW)	1.22 (0.08)	1.48 (0.08)	21 (9)
Thermal Efficiency (%)	23 (1)	31 (1)	34 (6)
Combustion Efficiency (%)	95.9 (0.3)	98.95 (0.07)	3.2 (0.3)
CO (g/kWd)	18 (3)	1.7 (0.3)	-90 (20)
PM2.5 (mg/kWd)	1200 (200)	90 (20)	-90 (20)
BC (mg/kWd)	550 (40)	54 (6)	-90 (10)

1212

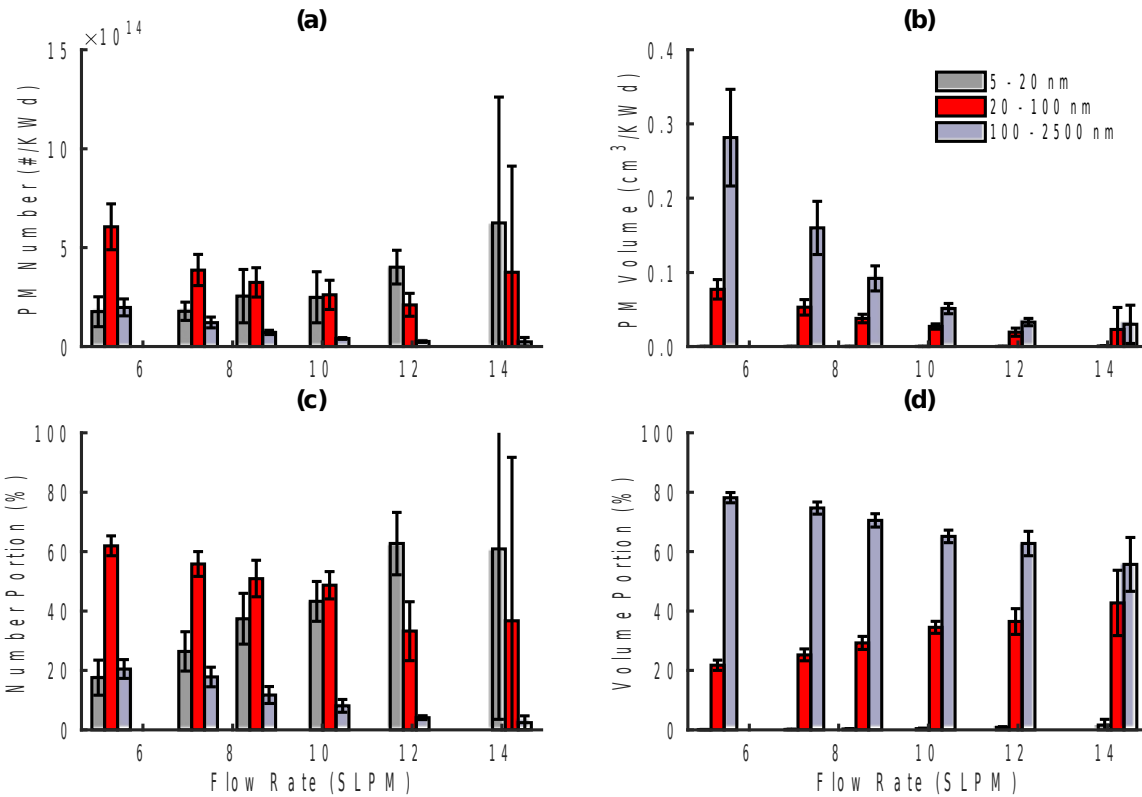
1213 **Table B1.** Performance and emissions metrics for a traditional three-stone fire (TSF) and the
 1214 MOD2 stove in the optimal configuration (air injection Pattern 2 at 12 SLPM). The mean and
 1215 90% confidence interval (in parentheses) are provided for each metric, and the corresponding

1216 number of replicate tests is indicated for each stove. The table also provides the percent change
1217 in MOD2 performance relative to the TSF.

1218

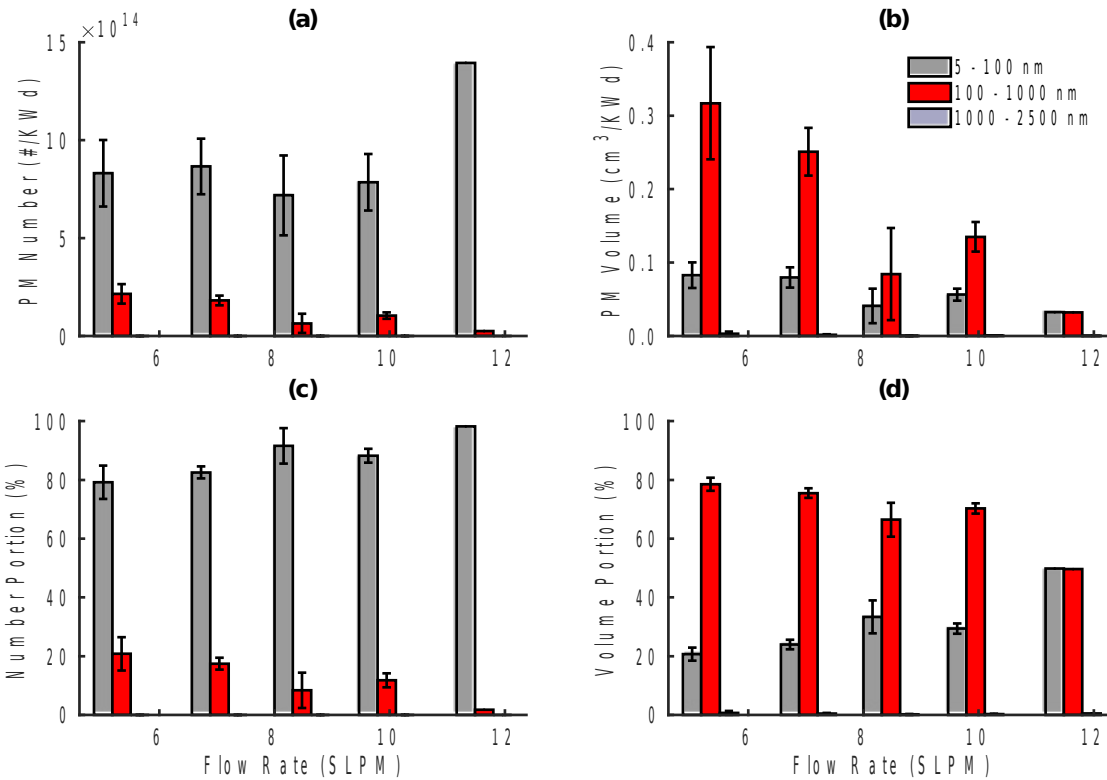
1219 **B.4 PM_{2.5} Generation: Additional Plots and Results**

1220 Size-resolved PM measurements were collected during parametric testing of air injection
1221 Pattern 2. For each secondary flow rate setting, Figure B5 presents the mean and 90% confidence
1222 interval of PM_{2.5} emission metrics from each set of replicate cold start tests. The metrics
1223 presented in Figure B5 are identical to that shown in Figure 4 except that the emission
1224 contributions from each particle size range have been rearranged such that confidence intervals
1225 can be displayed clearly. Figure B6 presents the same PM_{2.5} emission measurements as that
1226 shown in Figure 4 and Figure B5, but for three different size bins: 5 to 100 nm, 100 to 1000 nm,
1227 and 1000 to 2500 nm. This plot illustrates the emission of particles ranging from 100 to 1000 nm
1228 in diameter, which is not discernible in the other figures provided. Figure B7 and Figure B8
1229 present the same time-resolved PM_{2.5} accumulation measurements as that shown in Figure 5, but
1230 the data from the six parametric design configurations is split up over two Figures, such that 90%
1231 confidence intervals are clearly discernible. Only 2 tests were conducted at a secondary flow rate
1232 of 14 SLPM, and so the corresponding 90% confidence intervals are much larger than that shown
1233 at other secondary flow settings, for which 4 to 8 replicate tests were conducted.



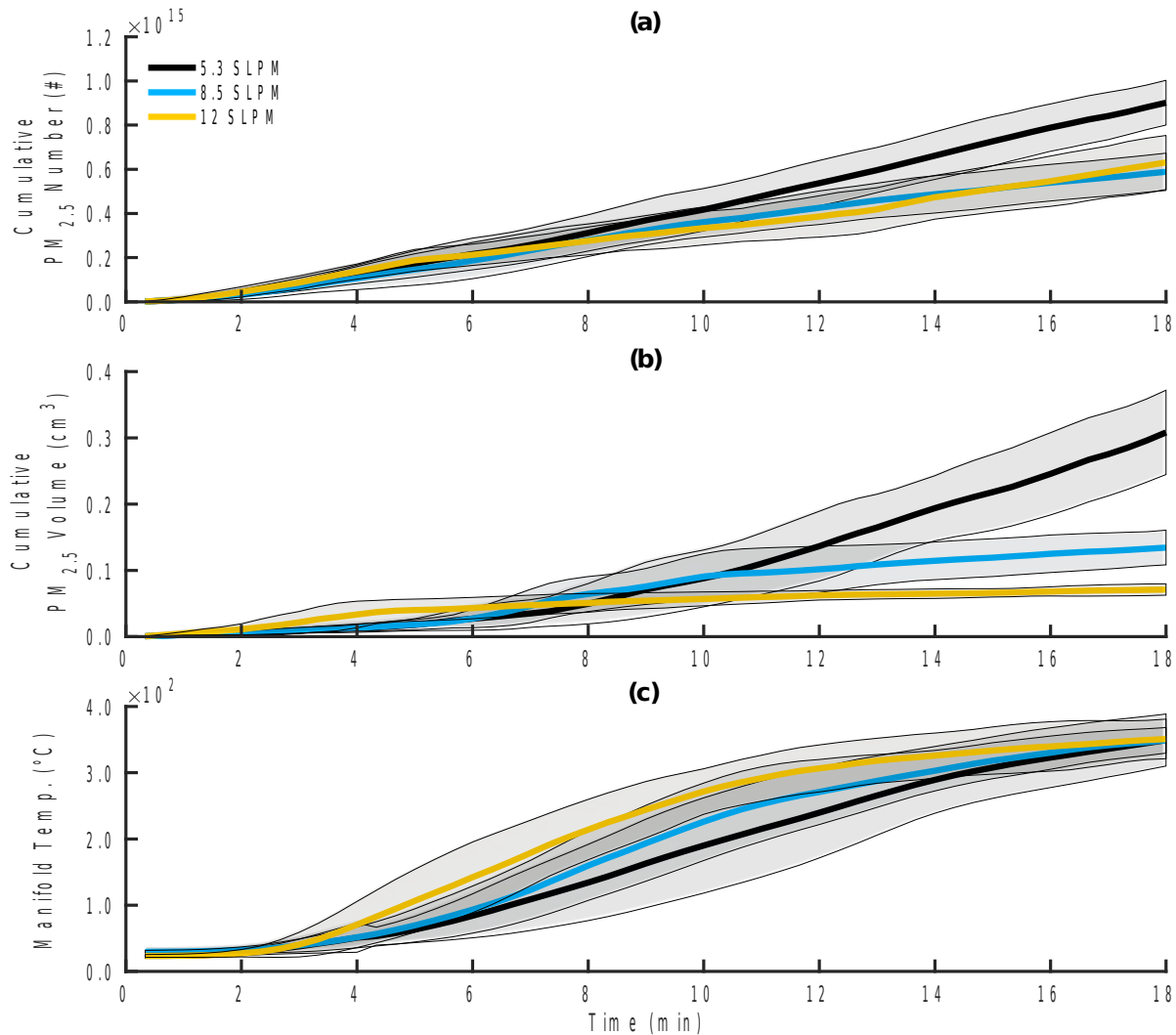
1234

1235 **Figure B5.** (a) Total PM_{2.5} number and (b) volume emissions from the MOD2 stove over the
 1236 cold start (normalized by cooking power), as a function of particle diameter and secondary air
 1237 flow rate through injection Pattern 2. (c) Portion of the total number, and (b) volume of particles
 1238 emitted in each particle diameter range: 5 to 20 nm, 20 to 100 nm, and 100 to 2500 nm. Each bar
 1239 represents the mean of replicate test data collected for each stove configuration, and error bars
 1240 represent the corresponding 90% confidence interval.



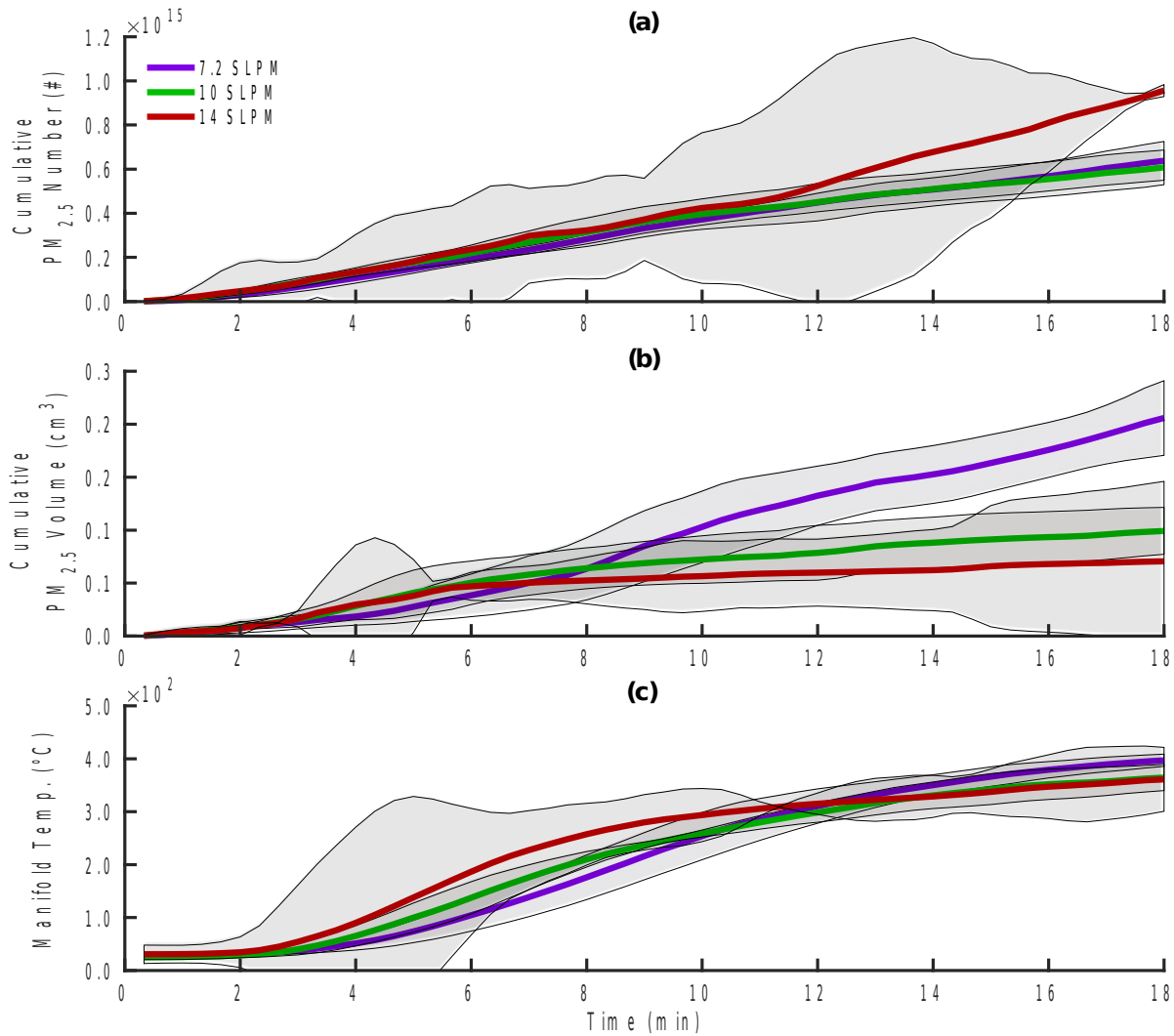
1241

1242 **Figure B6.** (a) Total PM_{2.5} number and (b) volume emissions from the MOD2 stove over the
 1243 cold start (normalized by cooking power), as a function of particle diameter and secondary air
 1244 flow rate through injection Pattern 2. (c) Portion of the total number, and (b) volume of particles
 1245 emitted in each particle diameter range: 5 to 100 nm, 1000 to 1000 nm, and 1000 to 2500 nm.
 1246 Each bar represents the mean of replicate test data collected for each stove configuration, and
 1247 error bars represent the corresponding 90% confidence interval.



1248

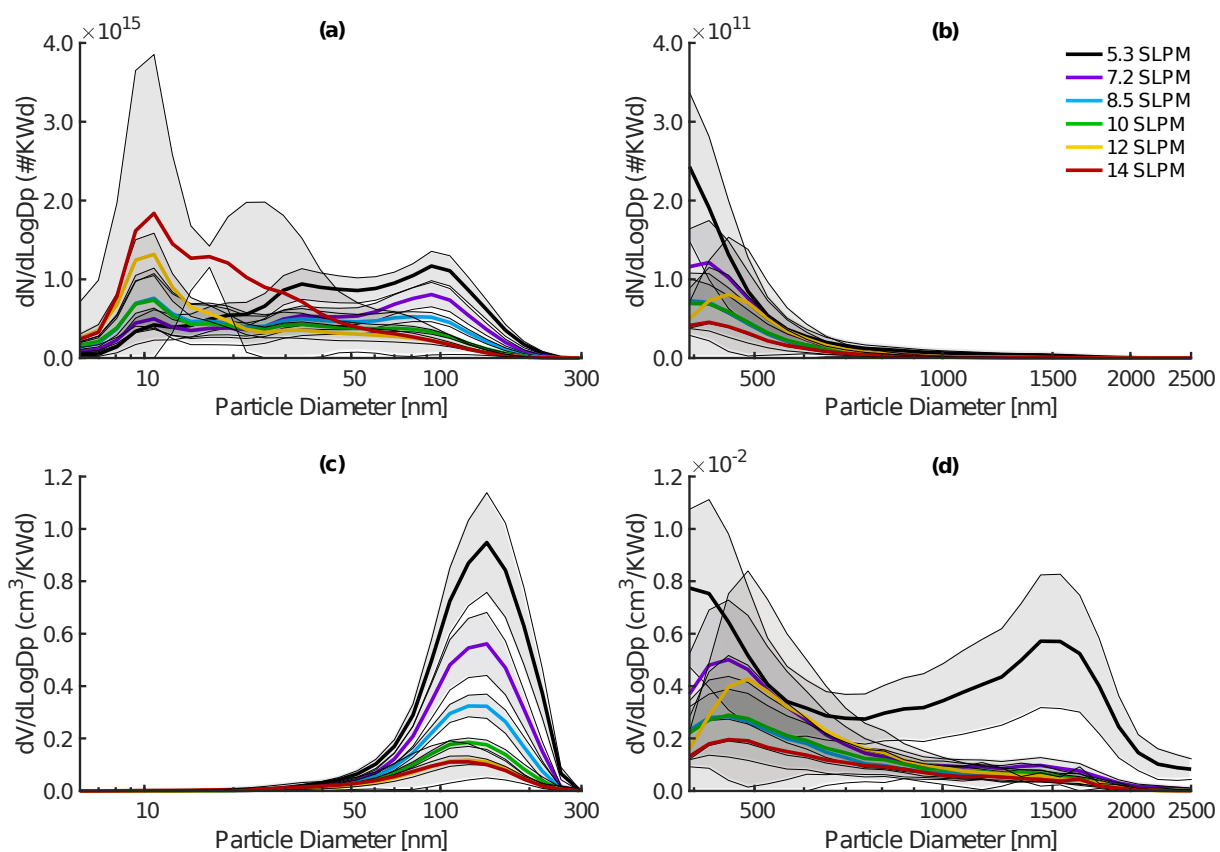
1249 **Figure B7.** (a) Accumulation of PM_{2.5} number and (b) volume emissions from the MOD2 stove
 1250 over the first 18 minute of the cold start. (c) Temperature of secondary air in the MOD2 stove
 1251 manifold over the same time period. Each bold line represents the mean of replicate test
 1252 measurements collected at secondary flow settings of 5.3, 8.5, and 12 SLPM (using air injection
 1253 Pattern 2), while shaded areas represent the corresponding 90% confidence interval. All data
 1254 presented is block-averaged on a 20-sec time base.



1255

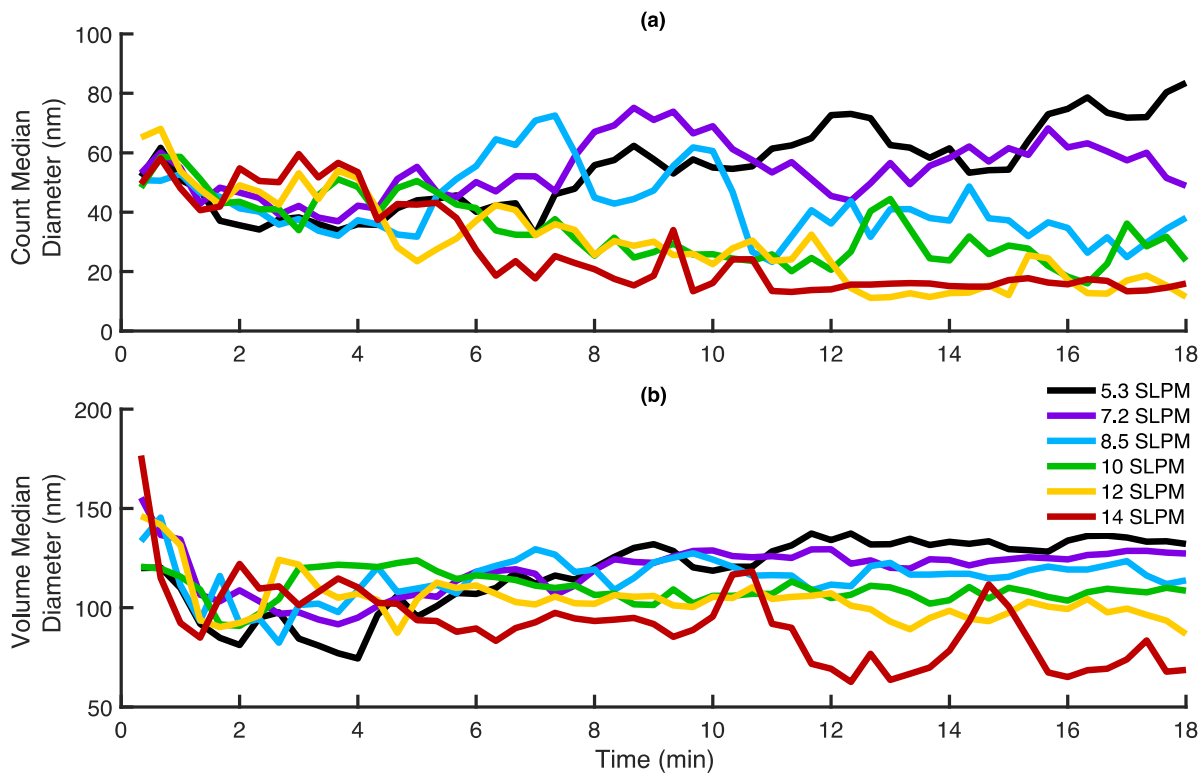
1256 **Figure B8.** (a) Accumulation of PM_{2.5} number and (b) volume emissions from the MOD2 stove
 1257 over the first 18 minutes of the cold start. (c) Temperature of secondary air in the MOD2 stove
 1258 manifold over the same time period. Each bold line represents the mean of replicate test
 1259 measurements collected at secondary flow settings of 7.2, 10, and 14 SLPM (using air injection
 1260 Pattern 2), while shaded areas represent the corresponding 90% confidence interval. All data
 1261 presented are block-averaged on a 20-sec time base.

1262 For each secondary flow rate setting, Figure B9 provides the size distributions of the total
 1263 $PM_{2.5}$ number and volume emitted by the MOD2 stove during the cold start. Figure B10 shows
 1264 the count median diameter (CMD) and volume median diameter (VMD) of $PM_{2.5}$ emissions over
 1265 the first 18 minutes of the cold start. Figure B11 and Figure B12 present the same time-resolved
 1266 median particle diameter data as that shown in Figure B10, but include the corresponding 90%
 1267 confidence intervals at each stove configuration.



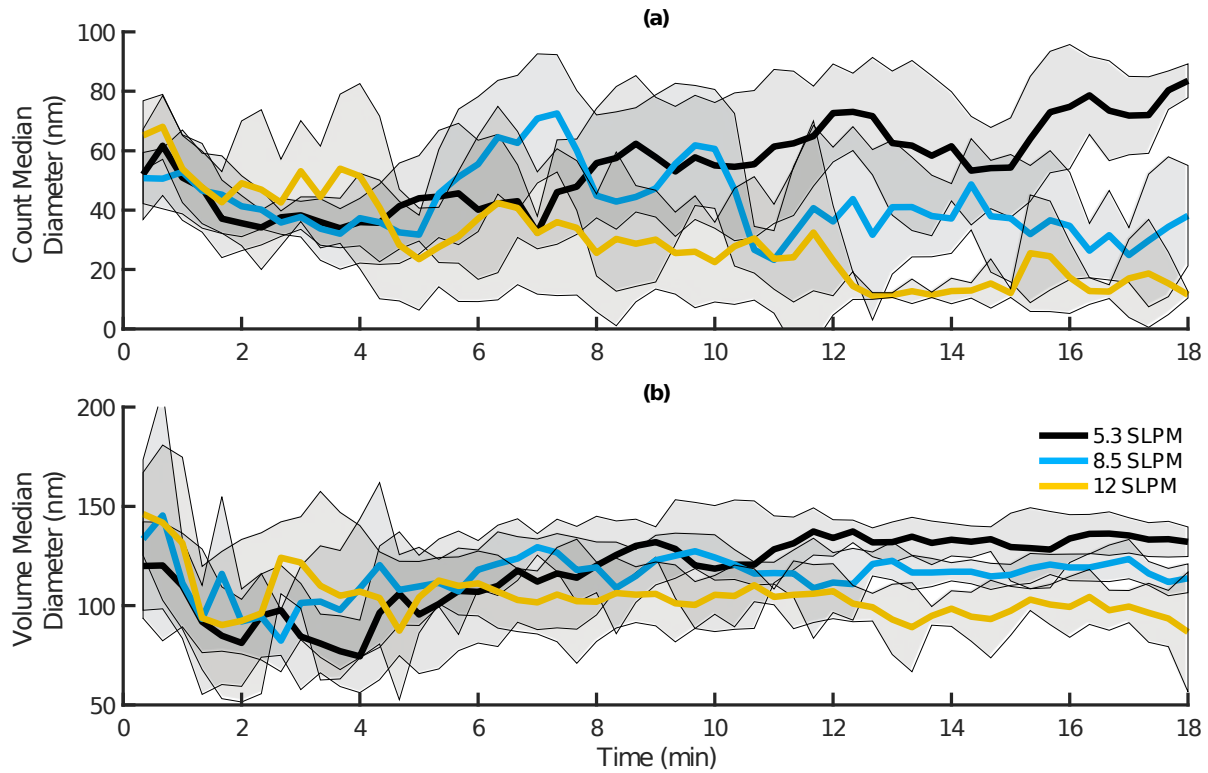
1268
 1269 **Figure B9.** Size-resolved distribution of total particle number or volume emitted during the cold
 1270 start, normalized by the average cooking power, for each secondary flow rate setting (using
 1271 injection Pattern 2): (a) FMPS particle number distribution; (b) APS particle number distribution;
 1272 (c) FMPS particle volume distribution; (d) APS particle volume distribution.

1273



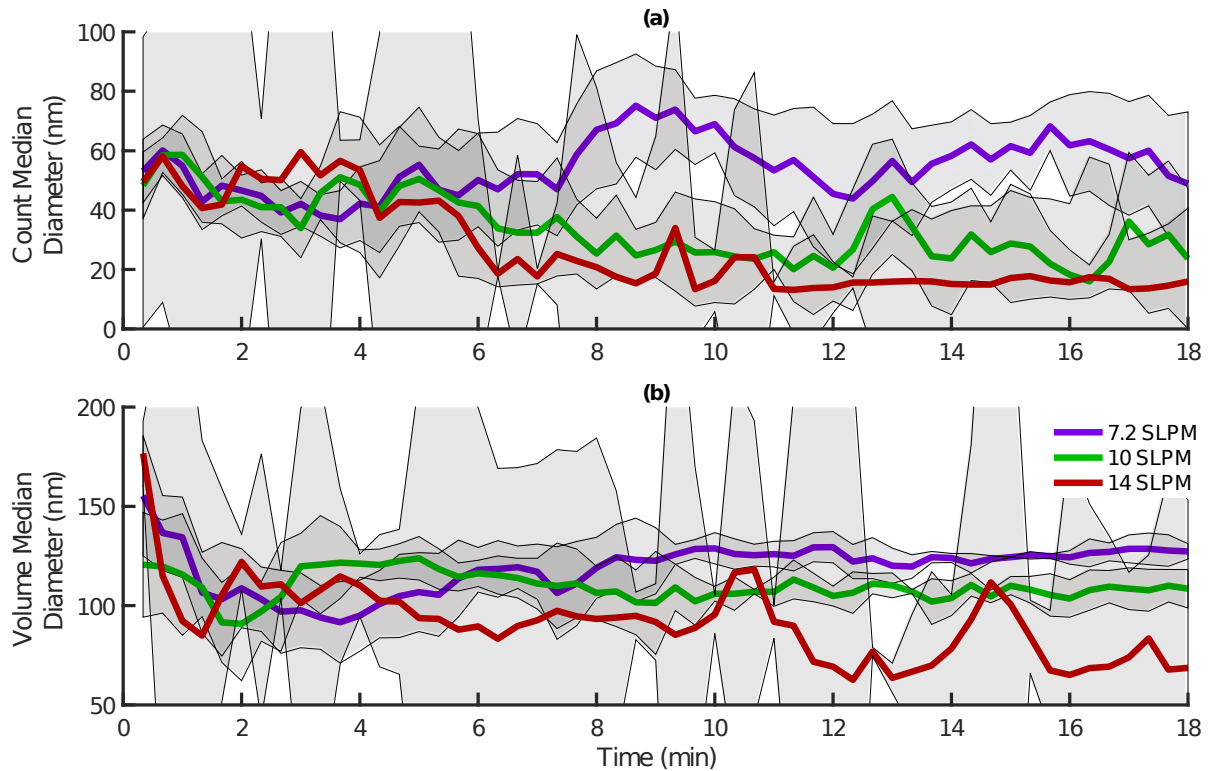
1274

1275 **Figure B10.** (a) Count median diameter and (b) count volume diameter of PM_{2.5} emissions from
1276 the MOD2 stove over the first 18 minutes of the cold start. Each line represents the mean of
1277 replicate test measurements collected at each of the six secondary flow rate settings (using
1278 injection Pattern 2). Confidence are omitted here for clarity, and instead provided in Figure B11
1279 and Figure B12 for all secondary flow rate settings. All data presented are block-averaged on a
1280 20-sec time base.



1281

1282 **Figure B11.** (a) Count median diameter and (b) count volume diameter of PM_{2.5} emissions from
 1283 the MOD2 stove over the first 18 minutes of the cold start. Each bold line represents the mean of
 1284 replicate test measurements collected at secondary flow rate settings of 5.3, 8.5, and 12 SLPM
 1285 (using air injection Pattern 2), while shaded areas represent the corresponding 90% confidence
 1286 interval. All data presented are block-averaged on a 20-sec time base.



1287

1288 **Figure B12.** (a) Count median diameter and (b) count volume diameter of PM_{2.5} emissions from
 1289 the MOD2 stove over the first 18 minutes of the cold start. Each bold line represents the mean of
 1290 replicate test measurements collected at secondary flow settings of 7.2, 10, and 14 SLPM (using
 1291 air injection Pattern 2), while shaded areas represent the corresponding 90% confidence interval.
 1292 All data presented are block-averaged on a 20-sec time base.

1293 B.5 Fan and Blowers Analysis

1294 On September 21, 2018, performance ratings and pricing information were downloaded from the
 1295 Digi-Key Electronics ® website for 2,273 fans and blowers.⁵⁰ All devices costing more than \$10
 1296 per unit (at an order quantity of 1000 units), rated for >10 W of electrical power consumption, or
 1297 missing a classification (blower vs. fan) were removed from the set, leaving 1,135 devices
 1298 remaining for analysis. The static pressure, free flow rate, and rated electrical power

1299 consumption of these 1,135 miniature axial fans and centrifugal blowers is depicted on Figure 3.
1300 This data is also provided in the attached Excel file entitled 'Fans_and_Blowers.xlsx', along with
1301 the corresponding model number, pricing, and other relevant information for each device.